Playa-Lunette System Mapping and Characterization in the High Plains of Western Kansas

By
© 2020
Melissa M. Goldade
B.S., University of Wisconsin-La Crosse, 2013

Submitted to the graduate degree program in Geography and Atmospheric Science and the Graduate Faculty of the University of Kansas in partial fulfillment of the requirements for the degree of Master of Science

_____
Co-Chair: Stephen L. Egbert, Ph.D.

_____
Co-Chair: Jude H. Kastens, Ph.D.

_____
William C. Johnson, Ph.D.

Date Defended: July 8, 2020

The Thesis Committee for Melissa M. Goldade certifies that this is the approved version of the following thesis:

Playa-Lunette System Mapping and Characterization in the High Plains of Western Kansas

_____
Co-Chair: Stephen L. Egbert, Ph.D.

_____
Co-Chair: Jude H. Kastens, Ph.D.

Date Approved: July 20, 2020

Abstract

Playa-lunette systems (PLSs) are common landscape features in the Great Plains that have been investigated from various perspectives including ecologic, geographic, hydrologic, and geologic. One of the region's most important water sources is the High Plains Aquifer (HPA), an expansive groundwater reservoir located beneath the PLSs, which has been susceptible to groundwater shortages, water table declines, and pollution throughout much of the High Plains due primarily to anthropogenic influences. This investigation takes on a new perspective, that of the geomorphology of playa basins and associated lunettes using LiDAR in a GIS environment. Playa-lunette systems were mapped using an objective method, or the largest closed contour (LCC) method, and a subjective method, also known as the subjectively chosen contour method (SC), with contours derived from a high-resolution LiDAR DEM. Basic 2-D attributes, e.g., area, perimeter, and orientation, were computed for the PLSs. The basin and lunette locations are consistent (perpendicular and parallel long axes, respectively) with late Pleistocene-early Holocene northwesterly paleo-winds of the last glacial period, with lunettes commonly being located south to south-easterly of the basins. This dataset fills the need for the mapping of the basins and compares two mapping methods with contours generated from high-resolution data. The assumption is that the SC method produces a visually ideal dataset, but the cons are that it is subjective and it requires more knowledge of PLSs. The LCC method is objective and has a set criteria to follow, producing more consistent results. A subset of 40 ideal playa-lunette systems (out of the 104 study sites from Bowen et al., 2018) were selected for a directional trends analysis and other 2-D metrics. Overall, the LCC method was comparable to the SC method, though the LCC method had a slight overestimation of the features comprising the PLSs. The LCC method and SC method mapped playas more consistently with the same contour than

lunettes. A relatively high correlation was found with regression plots of long axial orientation values between pairs of the datasets, as well as t-test results showing that these results are statistically similar.

Acknowledgements

I would like to thank my advisors, Dr. William C. Johnson, Dr. Jude Kastens, and Dr. Stephen Egbert for their knowledge, help, and support throughout the years, as well as Dr. Mark Bowen for his research on playa-lunette systems. Thank-you to Jennifer Glaubius for her help with organizing my thesis proposal. I also want to acknowledge Dr. Keith Floyd, Dr. Linda Keeler, my parents, my sister Jenny, Rosie, and Cindy for their support. I would also like to thank my current employer for helping fund the last few years of my graduate studies.

Table of Contents

List of Tables

List of Figures

1 Introduction

1.1 Groundwater Issues in the High Plains Aquifer

Groundwater shortages, water table declines, and pollution exist throughout much of the High Plains due primarily to anthropogenic influences. One of the region's most important water sources is the High Plains Aquifer (HPA), an expansive groundwater reservoir located beneath parts of Nebraska, Kansas, Oklahoma, Texas, and other neighboring states (Gurdak and Roe, 2009). Monitoring the status of water levels, water quality, and sources and rates of groundwater recharge will help to ensure water availability for future use.

Water shortages are common throughout the region due to an increase in irrigation for agriculture and a decrease in precipitation (Gurdak and Roe, 2009), with a result of an increasing depth to groundwater (McGuire 2014). Groundwater recharge, a process by which water infiltrates the soil and percolates to the water table, is not currently sufficient to compensate for the amounts of water being extracted. About 97% of the groundwater pumped from the HPA is used for irrigation as of the year 2000 (Maupin and Barber, 2005) to support a growing national population. A substantial decrease in groundwater levels has occurred in southwestern Kansas and northern Texas (Gurdak and Roe, 2009) in response to crop irrigation through the expansion of center-pivot technology, which allows for increased production of water-demanding crops, such as corn and alfalfa, in a semi-arid region that formerly produced predominantly dryland wheat. There are more efficient irrigated farming techniques that could potentially reduce the demand on water from the HPA, such as sub-surface drip irrigation and limited irrigation strategies, but those methods are not yet fully utilized.

Water in the HPA is not only declining, but it is also affected by anthropogenic pollution. The products and byproducts of oil and natural gas extraction have contaminated groundwater

and can further damage the environment. Oil wells are becoming increasingly common above the HPA in northern Texas, southwestern Kansas, and central Kansas due to the adoption of hydraulic fracturing and other new extraction technologies. Chemical pollution from agricultural runoff and infiltration from center-pivot delivery systems, including pesticides, herbicides, and fertilizers, negatively impact groundwater quality (Gurdak and Roe, 2009; Gurdak et al., 2009), especially given that these chemicals are used year after year. Groundwater recharge occurs at different rates based on diffuse and direct percolation flow patterns (McMahon et al., 2006), environmental and anthropogenic factors (Gurdak et al., 2007), and location of infiltration (Scanlon and Goldsmith, 1997). Contaminants from slow paths could potentially contaminate groundwater in the future (Gurdak and Roe, 2009), so water quality is a long-term concern.

1.2 Playas and Lunettes

The majority of playas in the High Plains lie above the HPA, so quantifying their role in groundwater recharge is of high importance. Playas are endorheic basins with no groundwater influence, so the water inputs are limited to direct precipitation and watershed surface runoff (Haukos and Smith, 1994; Tiner, 2003) and water losses of evaporation and infiltration (Rosen, 1994). As a result, playas periodically function as wetlands due to the accumulation of water (which can vary from year to year) and the resulting anaerobic soil conditions. Soils within the playa depression typically consist of smectitic clays, which shrink and swell, and can be hydric depending on the temporal presence of water. When dry, the smectitic clays in the playa develop cracks which increase infiltration, whereas when wet the clays swell shut and the playa becomes an evaporative basin conducive for supporting wetland flora and fauna (Scanlon and Goldsmith, 1997).

Playas are widespread ephemeral wetlands and shallow lakes located throughout the central and southern Great Plains and have been defined as elliptical depressions typically less than a few acres in size (Sabin and Holliday, 1995; Bowen et al., 2010). They consist of a basin (depression), an annulus (sloped edge of the basin), and an interplaya region, which is the upland area between playas and includes the playa catchment (Bowen and Johnson, 2012). Less commonly, playas have an associated lunette, a raised arcuate-shaped aeolian landform typically consisting of wind-blown fine sand and silt (Arbogast, 1996; Holliday, 1997; Bowen et al., 2018). Of the more than 80,000 playas identified on the High Plains in the Playa Lakes Joint Venture (PLJV) database (pljv.org), typically only the largest and deepest playas have associated lunettes (Sabin and Holliday, 1995; Arbogast, 1996; Bowen and Johnson, 2012). Collectively, a playa and lunette are considered a playa-lunette system (PLS) (Bowen and Johnson, 2012).

PLSs tend to develop in carbonate-rich environments where evaporite bed materials slowly dissolve over time, becoming weaker and more porous, thus leading to sub-surficial collapse (Wood and Osterkamp, 1987) and are then affected, when dry, by aeolian processes--deflational activity which can shift the sediment during climatic dry periods to form the lunettes (Bowen and Johnson, 2012). Sediment was likely available for transport during much of the Holocene due to dry climatic conditions (Bowen and Johnson, 2015), which encouraged the formation of lunettes as a result of aeolian activity. Northwesterly glacial-age winds in the central High Plains (Ahlbrandt and Fryberger, 1980; Arbogast and Muhs, 2000; Bettis et al., 2003; Mason et al., 2011) resulted in the transport and accumulation of silty loess from the interplaya and playa basin to accumulate, forming lunettes (Bowen and Johnson, 2012).

1.3 Importance of Playa-Lunette System Study

Since European settlement, anthropogenic activities have resulted in degradation and sedimentation of PLSs, which have been altered with agricultural fields, roads, or terracing. Sedimentation occurs when a playa basin fills in with eroded or windblown soil material and sediment, typically a result of poor landscape management practices (LaGrange et al., 2011), especially in cropland without grass buffers (Bowen and Johnson, 2017; Bowen and Johnson, 2019). If of sufficient depth, sediment accumulation can nullify the effects of hydric soil shrink-swell, impacting levels and speed of infiltration within the playa (LaGrange et al., 2011). As a result, not all playas exhibit evidence of hydric soils at the surface and some no longer function as wetlands.

2 Objectives and the Study Area

Western Kansas's original land cover was primarily short grass prairie (Kuchler 1974), but now consists mainly of rangeland and cultivated farmland. The climate is semi-arid (Veregin, 2005), and soils of the uplands tend to be formed in fine, calcareous loess, except where sand dunes have formed (Halfen et al., 2012). Soils in the playa basins are hydric and typically include the Randall, Church, Pleasant, Lofton, and Ness series (Web Soil Survey). PLSs in Kansas are limited to the western half of the state due to differences in hydrology, landscape, and climate, and commonly occur on loess-mantled uplands absent of major fluvial activity. Spatially, the PLSs are distributed into three north-south oriented groups separated by valleys of major eastward-flowing rivers, the floodplains of which often consist of coarse-grained alluvium, not suitable for playa development. The largest playa depressions can be detected as deep as the Ogallala Formation and date back to the late Pleistocene; the topography translocated upward to the PLSs on the surface (Bowen and Johnson, 2012).

2.1 Previous Studies and Ancillary Datasets

The first attempt at mapping Kansas playa wetlands was that of the Johnson and Campbell (2004) database, which used SSURGO hydric soil data to map playas. To minimize mapped non-playa features (i.e., to remove the hydric soil footprints that likely did not represent playas), a filter was included to keep the features mapped in upland locations. A drawback of the filter was the existence of hydric soils in river valleys and draws, which appear as small linear features in the dataset. Also due to sedimentation, hydric soils are not always visible at the surface. A total of 9,700 to 10,000 playas were identified in this study.

The Johnson and Bowen playa database (2009) (available from the Kansas Data and Access Center website) consists of over 22,000 Kansas probable playa wetlands mapped by Bowen et al., (2010) (Figure 1). A manual digitization process was utilized for playa wetland delineation, using four consecutive years of aerial imagery from the National Agriculture Imagery Program (NAIP). More recently, 2-m high-resolution LiDAR data have become available for western Kansas and have been evaluated for playa basin and catchment mapping (Kastens et al., 2016).

In Kansas, lunettes were delineated at a total of 104 locations; there are currently 129 known lunettes (some sites had multiple lunettes), about 50 of which have been confirmed on-site (Bowen et al., 2018). Digital raster graphics (DRGs, resolution ranging from 1.5 m to 6 m) and a high resolution LiDAR digital elevation model (DEM) were used to 'heads-up' digitize the lunettes, utilizing the Bowen and Johnson (2009) playa wetland database to help determine possible lunette locations. Proximity to a large playa wetland, contour shape (i.e., elongate and crescentic), and closed contours helped determine whether a lunette was present. Emphasis was placed on choosing the largest closed contour that encompassed the lunette. Spatial 2-D

attributes were calculated in ArcMap using Calculate Geometry (perimeter, area) and Minimum Bounding Geometry (long axis length, short axis length, and orientation angle).

2.2 Objectives

The main thrust of this research was to map (using non-automated methods) the population of PLSs from Bowen et al., (2018) using contours derived from a high resolution LiDAR DEM. In this study, a smaller subset of the Bowen et al., (2018) data was ultimately chosen for further analysis and was mapped using an objective, largest closed contour method (an adaptation from the original study) and a subjective method of hand-selecting the desired contours. Playas were mapped as basins (rather than as wetlands), with a goal of mapping the entirety of the depression that corresponds with the lunette, as presented in Bowen et al., (2018). Statistics were then run to get the 2-D attributes of the features, and further analyses of long axial orientation (directional trends) were completed using two programs (ArcMap 10.x and Matlab).

The objectives of this research include:

1. Compare the efficacy of the objective method versus the subjective method.
2. Evaluate the effect of smoothing the contours on the attribute values (e.g., perimeter).
3. Determine the sufficiency of elliptical curve fitting for calculating orientation values compared to the Minimum Bounding Geometry tool (used in Bowen et al., 2018).
4. Describe interesting cases of PLSs seen while mapping using LiDAR.

It is important to explore new and different ways to map PLSs, especially given more readily available high-resolution data, such as LiDAR. This research focuses on non-automated methods of LiDAR mapping suitable for smaller populations. There are a number of different non-automated mapping techniques, each with different levels of prior knowledge required to execute them.

3 Methods

3.1 Mapping

PLSs were mapped using a high-resolution LiDAR DEM (1 m horizontal resolution with a 95% confidence interval of ±9.5 cm on the vertical), supplemented with a hillshade DEM (2 m horizontal) and 0.25 m contour lines generated in ArcMap 10.x from the DEM, with the starting contour at 0 m. The 0.25 m interval was chosen because it allows for a highly refined contour set while also comfortably exceeding the 95% vertical confidence interval. A model created in ArcMap 10.x Model Builder was used to iterate through the dataset to clip the DEM and create localized areas of contours around the 104 PLS sites from Bowen et al., (2018) (as they are known locations of PLSs).

After the PLSs were mapped (Figure 2), a subset of 40 (a statistically useful sample size that allows for attention to individual cases) of the most ideal (elliptic and crescentic shapes for playas and lunettes, respectively) PLSs were selected (Figure 3). An ideal playa includes minimal fluvial scarring (i.e., inflow channel, delta, or alluvial fan formation) along the boundary and an elliptical shape. Lunettes were preferred if they had crescentic boundaries with minimal road disruptions and clearly rose up from the surrounding landscape. The playas and lunettes were examined individually with a binary standard and were given a score of ‘0’ for not ideal (do not include, examples in Figures 4 and 5) and ‘1’ for ideal (include). Each PLS had two values of either zero or one for each playa and lunette to determine which PLSs would be included in the subset. The resulting PLSs with values of ‘1’ in both categories were included in the subset. As the analyses for this study were to focus on directional trends, emphasis was placed on finding PLSs that had an ideal shape and would perform well when being fit to ellipses for the directional trends analysis.

The subset was mapped using two methods: the subjectively chosen contours (SC) method and the largest closed contours (LCC) method. The SC method represents the ideal way to map PLSs by going through the dataset on a case-by-case basis and choosing the contours best suited for each feature. Prior knowledge of typical PLS geomorphology was utilized in contour selection, e.g., aeolian dune geometry. Focus was that of finding a contour that represented the shape of the original feature, e.g., not including extra boundary alterations such as road cuts. The LCC method is a way to remove the subjectivity and to create a set of rules to achieve consistent, objective results and specifies that the largest closed contour around the feature is selected to represent that feature (similar to Bowen et al., 2018). Additional rules were applied as follows to identify a contour that better suited the feature in cases where the largest closed contour grossly overestimated the feature: 1) if a saddle point was included within the largest closed contour, the largest contour inside without the saddle point was chosen (Figure 6); and 2) if the contour was up against a road, then the largest contour inside the road was selected (Figure 7). In cases of saddle points where there were two topographic lows or highs, the most appropriate largest closed contour surrounding the largest (main) depression or topographic high would be chosen (Figure 8). Fluvial channels that affected PLS shape were not a determining factor when contours were selected.

ArcMap 10.x tools were used to clean up the datasets. Major boundary disturbances (e.g., due to fluvial activity and roads) were removed in both subsets to reduce noise in the ellipse-fitting (playas only) and directional trends (both playas and lunettes) results (Figure 9). The contours were originally classified as polylines, so the tool ‘Feature to Polygon’ was used to convert the polylines to polygons. Due to the complexity and sinuosity of the contours from which the polygons were generated, tiny polygon artifacts were created at some locations and

needed to be deleted (Figure 10). Playas with two main polygons (e.g., split due to roads, there were several cases in this dataset) were merged to be considered the same feature in the attribute table, but the boundaries were not physically combined (as it would not affect the orientation analyses) (Figure 11); the elevation value was consistent among the two polygons in each case. The 'Repair Geometry' tool was run (both before and after smoothing) to clean up any geometry errors caused by converting the polylines to polygons. Boundaries were then smoothed using the 'Smooth Line' tool, employing the PAEK algorithm with a tolerance of 20 m (ESRI – Smooth Line) to clean up the small scale variability of the lines. Smoothing the polygons too much could remove important shape detail, so a minimally sufficient value was sought. Values of 10, 20, and 50 m were tested to find no noticeable difference in the resulting perimeter values and, based on visual preference, 20 m was ultimately chosen. Due to rough boundaries, topology errors were flagged when running the smoothing tool due to tiny polygons on or just within the edge of the main polygon; these errors were fixed in the smoothed datasets (only a few features were flagged with topology errors) (Figure 12). Playa ID (PID) and LID (Lunette ID) fields were added to the databases to match the site numbers in Bowen et al., (2018). Using the 'Calculate Geometry' tool, the Area (m^2 and hectares) and Perimeter (m) were derived. The 'Minimum Bounding Geometry' (MBG) tool generated variables of width, length, and orientation, among others.

3.2 Directional Trends Analysis

Directional trends were analyzed for both playas and lunettes. For playas, the long axial orientation angle was calculated two ways: 1) MATLAB code utilizing the 'fit_ellipse' function (Gal, 2003), and 2) the MBG tool in ArcMap 10.x as in Bowen et al., (2018). The long axial orientation of the lunettes was calculated only using ArcMap 10.x tools, as the crescentic shape

data would be noisier when fit to ellipses. The resulting attributes of the same 40 lunettes in the subset mapped in this research and in Bowen et al., (2018) were compared.

For the first method, the MATLAB code fit_ellipse (Gal, 2003) was used to identify the best-fit ellipse, which utilizes the least squares method to find the ellipse with the lowest root mean square error, or RMSE when compared to a representative set of sample points from the playa boundary (Figure 13). Resulting attributes were long axis length, short axis length, and orientation. In preparation for the MATLAB code, the nodes were densified to 20 m in ArcMap 10.x to provide a dense, fairly uniform sample representation of the playa perimeter, as the edited areas with removed artifacts (e.g., a fluvial inlet branching into a playa) contained node gaps that affected the optimization. There were initially issues with the multi-polygons (due to roads splitting the features) when generating the outcome images after running fit_ellipse, as the vertices were read in as one long list; this was remedied by merging the polygons in the attribute table. The tool 'Feature Vertices to Points' with the 'All Points' option was used to convert the vertices to nodes, which were then inserted into the Matlab code.

For the second method, to calculate the directional orientation using ArcMap 10.x tools, 'Calculate Geometry' was used to calculate Perimeter and Area, and the MBG tool was used to calculate long axis length, short axis length, and orientation (as it was in Bowen et al., 2018). The 'convex_hull' polygon output option was chosen for the MBG tool given that it was able to most closely match the features' shapes (Figure 14). The fit_ellipse orientation scale was used as a default and the MBG orientations were converted to match using the equation: 90 – x (Figure 15).

3.3 Statistics

Plots and histograms were created in Matlab. Playa (MBG and fit_ellipse) and lunette (Bowen et al., (2018) and this research) long axial orientation were plotted via histogram. Linear regression plots were created for lunette and playa area and their respective long axial orientations, playa vs. lunette long axial orientation, and the corresponding playa (fit_ellipse and MBG) and lunette (Bowen et al., (2018) and this research) long axial orientations.

Circular variance (a method to indicate clustering in circular populations, e.g., directionality of the long axis of an ellipse) was calculated using the following equations (Allen and Johnson, 1991),

$$\mathrm{Var}(\theta) = 1 - \frac{R}{n} \qquad R^2 = \left(\sum_{i=1}^{n} \cos\theta_i\right)^2 + \left(\sum_{i=1}^{n} \sin\theta_i\right)^2$$

where n is the number of values being considered, theta (θ) is the long axial orientation angle, resulting values closer to 0 indicate highly similar angles (minimum variability), and resulting values closer to 1 indicate uniformly distributed clusters of angles across the full circular range (maximum variability); note: this distribution spans over half the circular range, from 90° to -90° (Figure 16).

T-tests were calculated on the major axial orientation values in Microsoft Excel using the 'ttest' function. The assumptions were two-tailed and homoscedastic (same variance between two different datasets) and the null hypothesis was that there was no significant difference between the datasets; the alpha value was set to 0.05, as that is a standard value.

4 Results

This research considered 13 datasets, including 8 playa and 5 lunette (see list below).

Playa

- Playa OS (MBG)
- Playa OSs (MBG)
- Playa SS (MBG)
- Playa SSs (MBG)
- Playa OS (fit_ellipse)
- Playa OSs (fit_ellipse)
- Playa SS (fit_ellipse)
- Playa SSs (fit_ellipse)

Lunette

- Lunette OS (MBG)
- Lunette OSs (MBG)
- Lunette SS (MBG)
- Lunette SSs (MBG)
- Lunettes – Bowen et al., (2018) (MBG)

The differences between the datasets are the method for calculating orientation (in parentheses), whether the dataset was smoothed (lowercase 's'), and whether the polygon delineations comprising the dataset were objectively selected or subjectively selected (OS vs SS).

4.1 Qualitative Results

For the binary classification of the PLSs, the playa and lunette pairs were each given a score based on whether the playa and lunette were considered 'ideal' to include in the dataset (zero indicating not ideal and one indicating ideal). Eight PLSs received a score of zero, 56 PLSs received a score of one, and 40 PLSs received a score of two (Table 1). Some PLSs were interchangeable - there were playas that were close to being included or could have been included; favor was given to those that best represented ideal examples of PLSs, focusing on shape and orientation (as the general orientation is known based on previous studies). Of the eight PLSs that had a score of zero, two were in Cheyenne County, one was in Wallace County,

two were in Scott County, one was in Lane County, one was along the Scott/Finney border, and one was in Morton County. Considering the playas and lunettes individually, 71 out of 104 (~68%) playas were given a value of '1'and 65 out of 104 (~62.5%) lunettes were given a value of '1'.

A total of 40 PLSs received a score of two and were included in the subset. Of the chosen subset, the majority of PLSs were in Scott, Lane, Finney, and Gray counties, similar to the distribution of the original Bowen et al., (2018) dataset, with exception to only one sample from the northwestern counties and lower inclusion of playas in Scott County and Finney County (Table 1). A number of the playas in Scott County and Finney County were close together and were not as distinct when compared to the surrounding landscape. Many ideal PLSs were in Lane County, which corresponds with the highest population of PLSs. As a whole, modified PLSs (by either anthropogenic means or by natural processes) were noted, but likely were not used in the subsets, e.g., for playas this includes boundaries altered by fluvial channels and playas that have been altered anthropogenically, e.g., with retention ponds and cultivation. The ideal shape and orientation of these playas can be surmised, but it is not always obvious and adds subjectivity. Modification for lunettes included road influences. The 40 chosen PLSs were mapped twice, using the LCC method and SC method, creating the OS and SS datasets, respectively.

4.2 Quantitative Results

4.2.1 Mapping

Playas were more commonly mapped with the same contour in the OS and SS datasets versus lunettes, and the OS dataset tended to have larger (in area) contours than the SS dataset for both playas and lunettes. Between the OS and SS datasets, 28 playas and seven lunettes had the same contour chosen for both datasets out of 40 total sample sites (Table 2). Of the 12 playas

where a different contour was chosen, all 12 had a larger contour chosen in the OS, which is the generally expected outcome whenever there is a difference. Nine of the 12 had a difference of one meter or less (four or fewer contours) and three playas had larger differences of seven, nine, and 15 contours. Contour shapes in these cases were similar, indicating that a smaller contour was not chosen to get a more precise shape in these cases; rather, a smaller contour was likely chosen while taking the landscape as a whole into context (i.e., a smaller contour was chosen because a deeper part of the depression was deemed to better suit the playa). Of the 33 lunettes where a different contour was chosen, 32 had a larger contour chosen, and one had a smaller contour chosen in the OS. In the instance of the larger lunette in the SS, the contour chosen for the SS was 0.25 m larger than the contour chosen for the OS. A smaller contour was chosen for the OS due to a road bordering the edge of the lunette (Figure 17).

The LCC method tended to produce larger (more expansive) boundary estimates versus the SC method. On average, the contours chosen for delineating the OS playas were about 0.3 m higher than the SS playas (the contours for this research were generated 0.25 m apart, so that would equal just over one contour) (Table 3). When considering the contours where the OS and SS datasets were in disagreement, the number increased to about 1 m (four contours). For lunettes, the average elevation difference was 0.75 m lower (three contours) between the OS and SS datasets, and about 0.9 m lower (between three and four contours) difference when only factoring in cases with differing contours. Regarding the OS – SS calculated difference values, the playa values were positive while the lunette values were negative; a smaller contour for lunettes has a higher elevation, whereas a smaller contour for a playa would have a lower elevation, resulting in positive values for playas and negative values for lunettes when subtracting the SS from the OS.

4.2.2 Metrics

Area, perimeter, short axis length, long axis length, and long axial orientation were calculated for the PLSs, similar to that of Bowen et al., (2018) with the lunettes. Among the four fit_ellipse playa datasets (OS, OSs, SS, SSs), the minimum long axis angle ranged from -0.8° (SSs) to -4.2° (OS) (Table 4). Maximum long axis angle in the four datasets was pretty consistent, between 34.3° and 35.3°. The mean long axis angle for the fit_ellipse playas was 15.3° for OS and OSs and 14.8/14.9° for SS and SSs. Standard deviation of the OS long axial orientation was 10.7° (OSs) and 11.0° (OS), whereas the standard deviation of the SS long axial orientation was 9.9° (SS) and 9.7° (SSs). Minimum long axis length for the four fit_ellipse playa datasets (OS, OSs, SS, SSs) were the same for both the OS and SS datasets at 567.4 m and the OSs and SSs datasets at 587.6 m (the same contour was chosen in both the OS and SS; likewise for the OSs and SSs). Similar results were seen with the maximum long axis length with playa 36 with values of 3556.2 m for OS and SS and 3576.7 m for OSs and SSs, though this playa seems to be an outlier. The next longest major axis was on playa 73, at about 2433 m, over 1,100 m shorter.

For the MBG playa results, the minimum long axial orientation was -11.3/-11.4° for the OS and OSs and -10.0/-9.9° for the SS and SSs (Table 5). The maximum MBG long axial orientation was around 55.5/55.7° for the OS and OSs and was 42.3° for the SS and SSs datasets. The mean MBG long axial orientation was 14.3/14.4° for OS and OSs and 12.6/12.7° for SS and SSs. The average for the fit_ellipse playa long axial orientation was 15.3° (Table 4) for the OS and OSs and 14.3/14.4° for the OS and OSs MBG playa long axial orientation.

Among the four MBG lunette datasets (OS, OSs, SS, SSs), the minimum long axis angle ranged from -1.0° (OS) to 5.0° (SS) (Table 6). The maximum long axis angle ranged from 63.3

and 63.5 in the SS and SSs to 89.4 in the OS and OSs. It does not appear that smoothing affected the maximum long axis angle in the OS dataset, but the minimum values in the OS and the maximum value in the SS were affected by smoothing by a factor of 0.2-0.3°. There was a six degree difference between the OS and SS lunette minimum orientation value and a 26 degree difference between the maximum long axial orientation values. The mean long axis angle for the MBG lunettes was 33.7 for OS and OSs and 30.9/31.4 for SS and SSs, which are comparable values. The standard deviation of the OS long axial orientation was 19.2 (OS) and 19.3 (OSs), whereas the standard deviation of the SS long axial orientation was 14.0 (SS) and 13.7 (SSs). The minimum long axis lengths for the four MBG lunette datasets (OS, OSs, SS, SSs) were the same for both the OS and SS datasets at 278.5 and the OSs and SSs datasets at 274.5. Differences were seen with the maximum long axis length with values of 2216.1 for OS, 2012.9 for SS, 2012.2 for OSs, and 2010.3 for SSs.

4.2.3 Smoothed vs. Non-smoothed

The contours were smoothed prior to analyses to examine whether smoothing was effective for cleaning up the inflated perimeter values due to sinuous boundaries, as large values were seen in the OS and SS datasets, or if it was better suited for visual/aesthetic purposes. The goal was to maintain the detail in the datasets, but also to not have larger than realistic perimeter values. Based on the resulting attributes, the perimeter values decreased significantly due to smoothing the contours. The SS values tended to overestimate perimeter statistics when compared to Bowen et al., (2018), while the SSs values tended to underestimate (Table 9). Smoothing did not appear to substantially affect the other metrics. The standard deviation was lower in the smoothed datasets. The maximum and minimum values better matched those in

Bowen et al., (2018) for the SSs lunettes, though the SS values were better matched for the median and mean.

4.2.4 Circular Variance

Circular variance values ranged between 0.02 and 0.05 (Table 10). Overall, results showed intense clustering and a tight range of orientation values. In terms of smoothing's effect on orientation angle distribution, the largest difference in circular variance values between the smoothed and unsmoothed datasets was seen in SS lunettes with a difference of 0.001, indicating that the SSs lunette dataset had more clustering and tighter orientation range than the SS lunette database. Otherwise, smoothing had minimal effect on circular variance values. OS playas and SS playas had a difference of 0.01. SS playas had a slightly tighter orientation range and the values were more clustered. This could be in part caused by the SS playas tending to have smaller contours, which may have less large-scale variation than larger contours. The OS lunette circular variance value was 0.025 higher than the SS lunette circular variance value, indicating that the SS lunettes had a closer range of orientation values and clustering. Of the 40 sites, 32 sites had larger contours in the OS lunette dataset. Similar to the playa databases, the smaller contours may better capture the orientation angle and be less subject to natural or anthropogenic boundary alterations.

4.2.5 Directional Trends Analysis

The playa SS MBG long axial orientation and the playa fit_ellipse long axial orientations were both most commonly between 0° and 45° (Figures 18 and 19). No playas in the subset had long axial orientations past -45°. The MBG results had values closer to 0°, while the fit_ellipse results had values skewed more to the right (or closer to 45°). Correlation between the fit_ellipse and MBG data was fairly strong correlation at 0.7 (Figure 20). Plotting OS playa and SS playa

long axis orientations had pretty clean results, with only four outliers (Figure 21). The lunette results were messier, which was partly attributable to the fact that a larger number of playas were mapped with the same contours in both the OS and the SS (Figure 22).

To quantify and compare ellipse eccentricity for the MBG and fit_ellipse methods, the minor axis length was divided by the major axis length for the SS MBG dataset (Figure 23) and the SS playa fit_ellipse dataset (Figure 24). Both samples appeared to be approximately normally distributed, but the MBG data had a more bell-shaped appearance. Both datasets had a similar mean. The average value of the minor axis length divided by the major axis length was between 0.55 and 0.6, indicating that most of the minor axes were just over half of the length of the major axes; ellipses with a minor/major value near zero would be very elongated, whereas those with a value of 1 would be a circle (same length). The fit_ellipse data were denser around 0.7 and 0.8, indicating that the ellipses fit toward some of the features were more circular. Also the bulk of the data was slightly skewed around 0.5 in the fit_ellipse with fewer data points in the 0.6 bin. There was a more even range in ellipse shape in the MBG dataset versus in the fit_ellipse dataset.

Both lunette area and perimeter had a weak negative correlation with long axial orientation (Figures 25 and 26), indicating that lunettes of a certain size are not more likely to have a particular orientation. Both playa area and playa perimeter are not correlated with playa orientation (ArcMap SS playa results) (Figures 27 and 28). The correlation is even less than for the lunettes, likely because lunettes have a more distinct, oblong and crescentic shape, while playas tend to be more circular, making it more difficult to get high-confidence orientation results. When examining the long axial orientation of the SS playas versus the SS lunettes, there was a weak correlation of 0.31 (Figure 29).

The LCC method results and SC method results appear to be statistically similar. T-tests were used for statistical analyses because histograms of the data revealed approximately normal-looking distributions. The results of the four t-tests show that the differences between the pairs of datasets (OS Playa (MBG) and SS Playa (MBG), OS Lunette (MBG) and SS Lunette (MBG), SSs Playa (MBG) and fit_ellipse, and SSs Lunette (MBG) and Bowen et al., (2018) (MBG)) compared are statistically insignificant (Table 11), indicating that the respective results could have come from either of the two populations compared in each scenario; i.e., the datasets are very similar. The p-values ranged from 0.42 to 0.60. Assumptions were that the test was two-tailed, homoscedastic (same variance between two different datasets), a null hypothesis of 'No significant difference between datasets', and an alpha of 0.05.

4.2.6 Comparison to Bowen et al., (2018) data

The dataset in Bowen et al., (2018) included 129 lunettes, but for comparison to this research, the corresponding 40 chosen for the subset were analyzed. Minimum area was 2.44 ha and the maximum area was 80.43 ha (Table 7). Long axis length ranged from 311 m to 2565 m and the long axial orientation ranged from 9.7° to 71.5°. Maximum OS lunette perimeter was 5522 m larger than Bowen's largest perimeter (Table 8). Smoothing the dataset brought that value down by about 4500 m. Maximum long axial orientation in the OS lunette subset was 17.9° greater than Bowen's maximum long axial orientation. Maximum SS lunette long axial length was 554.7 m longer than Bowen's maximum. SS lunette maximum perimeter was 1521.2 larger than Bowen's, but smoothing lowered that value to 987.8 larger than Bowen's.

When compared to the Bowen et al., (2018) lunettes, the MBG SS lunette perimeter values were higher, with a minimum perimeter value of 42% higher and a maximum perimeter value of 25% higher (Table 8). The median of the SS dataset and the Bowen et al., (2018) dataset

were nearly the same. The mean perimeter value was 9% higher in the SS dataset. Smoothing the MBG SS lunette database decreased the perimeter values by 29% for the minimum value and by 33% for the maximum value. When smoothed, the median perimeter was decreased by 25% and the mean perimeter was decreased by 27%. The MBG SSs lunette database had overall smaller perimeters than Bowen et al., (2018), with a minimum value 1% higher and a maximum perimeter value 17% lower. The median and mean were 25% and 21% smaller, respectively.

When comparing the long axial orientation for the lunette MBG SS (Figure 30) and the long axial orientation for the same 40 lunettes in the Bowen et al., (2018) subset (Figure 31), the highest frequency of orientations are between zero and 50°. The peak was around 30° for the SS data and 40° for the Bowen data. Bowen's lunettes were skewed to the left and clustered around 20, 30, and 40° whereas the SS data had more of a normal distribution with a peak at 30. The correlation was fairly strong at 0.8 (Figure 32).

5 Discussion

5.1 Mapping

At the beginning of the mapping process, subjectivities included the decision as to which contour best fit the feature, e.g., the largest closed contour, the contour at the outer edge of the playa annulus (wall), or the contour on the inner edge of the playa annulus (Figure 33). Digitizing the features 'heads-up' using the LiDAR DEM was attempted but was rather open-ended given the high resolution of the data, so a more objective method for determining boundaries was sought. This subjectivity demonstrates the need to find an objective method that is repeatable and reliable. Generating 0.25 m contours from the LiDAR data helped to decrease the subjectivity in the boundary delineation process by providing a boundary candidate library to choose from. From this, the features were subjectively mapped by a professional choosing the

so-called “best” contour according to their judgement (subjective contour, or SC), as well as objectively mapped using the largest closed contour (LCC; similar idea as used in Bowen et al., 2018), but with a few additional rules added.

As anticipated, using the DEM was effective for mapping the playa basins, since the features were not subject to noise from the variable land cover in the aerial photography. However, there were some aspects of the DEM that made mapping unclear. A con of the LCC method is when the playa boundaries as a whole are altered. There were cases where drainage channels going into the depression were included in the boundary, and where anthropogenically altered boundaries were mapped as the playa, e.g., in the case of agricultural retention ponds. The SC method could help in these cases if there were smaller contours that better represented the feature, but if all contours are affected then contour-based boundaries that represent the original feature shape might be difficult to obtain.

The crescentic shape was not utilized in this research as it was in Bowen et al., (2018). For this study, boundaries were not changed based on the crescentic-shaped criteria used in that paper; in some cases it may have helped clean up the boundaries that were too large, but then would run into the subjective question of 'which contour should be chosen?' as many of the contours are crescent-shaped and the best-suited one may not be the largest crescent. Also some of the dunes are rounded and are not appropriately described as crescentic. The data used in Bowen et al., (2018) were limited in some cases to the 1.5 m - 6 m resolution DRGs, given that LiDAR coverage in Kansas was not widely available at the time. Closely spaced contours generated from the LiDAR DEM helped the crescentic patterns in the landscape become more visible. Given the high-resolution and detail of the LiDAR DEM, possible unmapped lunettes

were located by their geographic location, close contour spacing, and crescentic shape (Figure 34).

The elevation differences between the playa and lunette were not considered as the landscape is not a flat plane, though that does raise the question to which boundaries best delineate the playas and lunettes (another factor that demonstrated a need for an objective mapping method). Some of the currently mapped lunettes had multiple high points, leading to a subjective decision of which and how many of those rises to map. Initially while mapping, it was questioned whether it would be best to try to match the contour from Bowen et al., (2018) or to map features exclusive of saddle points (i.e., the highest peak); ultimately the latter was chosen, leading to one of the additional rules of the LCC method.

The two additional rules of the LCC method (choosing the contour smaller in area than a road-affected contour and choosing the contour adjacent to the saddle point) did not always help narrow down the contours to that of the original landform. In particular, this applied to 'stretched' lunettes, whose boundaries seem large and exaggerated down the leeward (downwind) slope (Figure 35). Roads were not affecting the shape of the feature and there was no saddle point to give any indication as to where to cut the feature off. For the stretched lunettes, the features seemed over-mapped in area and the contours chosen in the SC method would have better suited the original feature.

5.2 OS vs SS

Generally, the objective method mapped the PLSs larger in area than the subjective method. At times, the objective method seemed to over-estimate the area of the PLSs (e.g., stretched lunettes or including extra lobes in the playa boundaries). Many times the playa or lunette were a part of a larger depression or ridge, causing the largest closed contour to

overestimate the feature's area. A modification to the largest closed contour method was the use of the saddle point to help determine the contour chosen, generally allowing the individual features to be better estimated. Also, the additional rule of choosing the largest closed contour inside of a road-affected boundary was implemented to help offset the overestimated boundaries that were caused by roads.

The OS and SS methods both seemed to be more consistent in mapping the playas versus the lunettes. It was much more common for the same contour to have been selected in both the SS playa database and the OS playa database versus those in the respective SS and OS lunette databases. This could indicate that it is easier to determine the boundary of a depression with contours versus the boundary of a protrusion (specifically, a dune). A case where the OS method did not work ideally for mapping lunettes includes stretched lunettes.

Results of the objective method are largely unbiased and repeatable, while the results of the subjective method are based on expertise and knowledge of PLSs, for which many professionals have a different definition (i.e., the question "what defines a playa?" is open to interpretation). This manual selection process can introduce subjectivity as to where to delineate the depression's boundaries. Knowledge of PLS geomorphology, local soil series, local topography, and fluvial processes will be necessary for mapping PLSs. Contours used in this research are 0.25 m apart and at times there may not be much variation between choosing surrounding contours. Other subjectivities include whether the contours are mapped around the inner or outer annulus and whether the boundary abnormalities (due to natural or anthropogenic influences) are sought to be included as a part of the feature.

Depending on the purpose of the study, either method could be justified. If generous (larger in area) boundaries would be preferred (e.g., to maximize the feature footprint for

conservation purposes), then the objective method could be used. Also, if the questions at hand are best addressed using a methodology that is consistent and repeatable (e.g., mapping the features throughout the entire Great Plains or multiple people with varying knowledge bases mapping the features), then the objective method would be preferred. To assess the shape and best estimate the geomorphic extent of the original feature, the subjective method might be utilized. Also, if the results are to precisely analyze the playas and lunettes (e.g., geometrically, morphometrically), the subjective method provides tighter contours that more closely match the topographical shape of the feature and seem to be less frequently affected by natural or anthropogenic boundary disturbances.

5.3 Matlab vs MBG

Given the analyses of both the LCC and SC methods, further analyses were desired to quantify 2-D metric results of both datasets. Elliptical fitting and a long-axial directional trends analysis were focused on in greater detail, including the two different methods of calculating this metric (fit_ellipse and MBG). One main difference between the fit_ellipse and the MBG methods are the way the features were fit to ellipses; the fit_ellipse function uses the least squares method to find the lowest RMSE while orienting the ellipse, while the MBG method creates an envelope around the feature, finds the longest distance between two points, and draws a line between them for the long axis (Figure 36).

The differences in long axial orientation results could be due to the fitting of the envelopes around the features in the MBG method. Extra fluvial channels, for example, would affect the shape of the playa and therefore the envelope. Convex shapes appear to fit best with the envelopes versus concave shapes; when the shape is concave, the envelope surrounds the entire feature, even if there is dead space in-between the boundary and the feature.

5.4 Metrics

The plot for OS vs SS MBG playa orientation included four outliers (Figure 20). The outliers were mapped with different contours for the OS and SS datasets (Figure 37). In two of the cases, extra lobes on the playas affected the overall shape of the envelope. In the other two cases, small fluvial channels affected the shape of the envelopes. These examples show a weakness of the MBG envelope-fitting method and could be a case for using the fit_ellipse least squares fitting method. Another example of an outlier was a lunette with a large area, perimeter, and 5° orientation located in Gray County. The corresponding playa is unique in that it is especially elongate. This case would be an anomaly with both the fit_ellipse and MBG methods.

For circular variance, the lunette and playa values were comparable, but the lunette values were slightly larger than the playa values. This could be due to the shape of the features. Playas tend to be more elliptical, whereas the lunettes tend to be more crescentic. The polygon drawn around the playas by the MBG tool would likely better match the playas with less empty space, giving a more accurate representation of that feature's long axis. The lunettes were not fit to ellipses using fit_ellipse for this reason.

5.5 Future Studies

The lunette database could be expanded given the full-state LiDAR coverage completed in the last few years. Future studies could try out a larger sample (perhaps all 104 sites in Bowen et al., 2018) with more complex cases to examine the effectiveness of the objective and subjective methods with a larger sample size. Cases in which the boundaries were heavily modified were not included in the dataset for this research.

Another interesting variable to evaluate would be the angle between the centroids of each playa and its lunette. The angles could be measured against the long axis of the playa, and the

angle at which the sediment was blown from the playa to the lunette could be estimated. This could be compared with previous studies of paleo-wind direction and used to provide more detail for western Kansas.

Future studies could look more into combining the repeatability of the LCC method and the ideal results due to the deliberately chosen contours of the SC method. Additional rules may need to be added to better narrow down the LCC method contours, e.g., choosing a contour within tightly clustered contour groups (quick elevation change over a small area) to help determine the contour closest to the edge of the feature.

6 Conclusions

A non-automated method to map PLSs objectively and to conduct geomorphic statistical analyses was sought. Utilizing the high resolution DEM contours removed the subjectivity of heads-up digitizing. Two valid methods were examined in this study to map PLSs. The LCC method has a repeatable, consistent methodology, which therefore removes much of the subjectivity. Overall, it seemed that the LCC method was comparable to the SC method. The objective method provides a slight overestimation of the PLSs, but provides a defined methodology that does not require as much background knowledge. Playas were more consistently mapped with the same contour in both methods versus the lunettes. Regression plots and t-tests on the long axial orientation values between pairs of the datasets showed that the results are statistically similar. In terms of applications of this research, the resulting playa datasets could be of use to conservationists, particularly those interested in wildlife ecology and habitat classification, and individuals in groundwater resource management, especially for studies in groundwater recharge during playa hydroperiods. The lunette databases could

potentially be of use to cultural resource experts to aid in the location of archaeological study sites.

References

Ahlbrandt, T.S., Fryberger, S.G., 1980. Eolian Deposits in the Nebraska Sand Hills. Geologic and Paleoecologic Studies of the Nebraska Sand Hills, US Geological Survey Professional Paper 1120, 1-24.

Arbogast, A.F., 1996. Late Quaternary evolution of a lunette in the central Great Plains: Wilson Ridge, Kansas. Physical Geography, 17(4), 354-370.

Arbogast, A.F., Muhs, D.R., 2000. Geochemical and mineralogical evidence from eolian sediments for northwesterly mid-Holocene paleowinds, central Kansas, USA. Quaternary International, 67(1), 107-118.

Allen, F.H., Johnson, O., 1991. Automated conformational analysis from crystallographic data. 4. Statistical descriptors for a distribution of torsion angles. Acta Crystallographica Section B, 47(1), 62-67.

Bettis, E.A., Muhs, D.R., Roberts, H.M., Wintle, A.G., 2003. Last glacial loess in the conterminous USA. Quaternary Science Reviews, 22(18), 1907-1946.

Bowen, M.W., Johnson, W.C., 2012. Late Quaternary environmental reconstructions of playa-lunette system evolution on the central High Plains of Kansas, United States. Geological Society of America Bulletin, 124(1-2), 146-161.

Bowen, M.W., Johnson, W.C., 2015. Holocene records of environmental change in High Plains playa wetlands, Kansas, US. The Holocene, 25(11), 1838-1851.

Bowen, M.W., Johnson, W.C., 2017. Anthropogenically accelerated sediment accumulation within playa wetlands as a result of land cover change on the High Plains of the central United States. Geomorphology, 294, 135-145.

Bowen, M.W., Johnson, W.C., 2019. Sediment accumulation and sedimentation rates in playas on the High Plains of western Kansas, USA. Geomorphology, 342, 117-126.

Bowen, M.W., Johnson, W.C., Egbert, S.L., Klopfenstein, S.T., 2010. A GIS-based approach to identify and map playa wetlands on the High Plains, Kansas, USA. Wetlands, 30(4), 675-684.

Bowen, M.W., Johnson, W.C., King, D.A., 2018. Spatial distribution and geomorphology of lunette dunes on the High Plains of Western Kansas: implications for geoarchaeological and paleoenvironmental research. Physical Geography, 39(1), 21-37.

ESRI. Minimum Bounding Geometry (Data Management). <https://pro.arcgis.com/en/pro-app/tool-reference/data-management/minimum-bounding-geometry.htm>. Accessed 25 February 2020.

ESRI. Smooth Line. <http://desktop.arcgis.com/en/arcmap/10.5/tools/cartography-toolbox/smooth-line.htm>. Accessed 3 September 2018.

Gal, Ohad, 2003. fit_ellipse. MATLAB Central- File Exchange. <http://www.mathworks.com/matlabcentral/fileexchange/3215-fit-ellipse>. Accessed 10 November 2015.

Gurdak, J.J., Hanson, R.T., McMahon, P.B., Bruce, B.W., McCray, J.E., Thyne, G.D., Reedy, R.C., 2007. Climate Variability Controls on Unsaturated Water and Chemical Movement, High Plains Aquifer, USA. Vadose Zone Journal, 6(3), 533-547.

Gurdak, J.J., McMahon, P.B., Dennehy, K., Qi, S.L., 2009. Water quality in the High Plains aquifer, Colorado, Kansas, Nebraska, New Mexico, Oklahoma, South Dakota, Texas, and Wyoming, 1999–2004. US Geological Survey Circular 1337, 63 p.

Gurdak, J.J., Roe, C.D., 2009. Recharge Rates and Chemistry Beneath Playas of the High Plains Aquifer--A Literature Review and Synthesis. US Geological Survey Circular 1333, 39 p.

Halfen, A.F., Johnson, W.C., Hanson, P.R., Woodburn, T.L., Young, A.R., Ludvigson, G.A., 2012. Activation history of the Hutchinson dunes in east-central Kansas, USA during the past 2200 years. Aeolian Research, 5, 9-20.

Haukos, D.A., Smith, L.M., 1994. The importance of playa wetlands to biodiversity of the Southern High Plains. Landscape and Urban Planning, 28(1), 83-98.

Holliday, V.T., 1997. Origin and evolution of lunettes on the High Plains of Texas and New Mexico. Quaternary Research, 47(1), 54-69.

Johnson, W. C., Bowen, M. W., and Klopfenstein, S., 2009, Kansas Playa Wetlands Digital GIS Database, Available online: <www.kansasgis.org>.

Johnson W.C., Campbell J.S. (2004). Playa lakes: Database of playa distribution in western Kansas. Data Access and Support Center, Kansas Geological Survey. No longer available online (superceded).

Kastens, J.H.**,** D.S. Baker, D.L. Peterson, and Huggins, D.G., 2016, Wetland Program Development Grant (WPDG) FFY 2013 – Playa Mapping and Assessment. KBS Report #186. Kansas Biological Survey, University of Kansas, Lawrence, 28 p.

Kuchler, A.W., 1974. A New Vegetation Map of Kansas. Ecology, 55(3), 586-604.

LaGrange, T.G., Stutheit, R., Gilbert, M., Shurtliff, D., Whited, P.M., 2011. Sedimentation of Nebraska's Playa Wetlands: A Review of Current Knowledge and Issues. Nebraska Game and Parks Commission, Lincoln, 62 p.

Mason, J.A., Swinehart, J.B., Hanson, P.R., Loope, D., Goble, R.J., Miao, X., Schmeisser, R.L., 2011. Late Pleistocene dune activity in the central Great Plains, USA. Quaternary Science Reviews, 30(27-28), 3858-3870.

Maupin, M.A., Barber, N.L., 2005. Estimated withdrawals from principal aquifers in the United States, 2000. US Geological Survey Circular 1279, 47 p.

McGuire, V.L., 2014. Water-level changes and change in water in storage in the High Plains aquifer, predevelopment to 2013 and 2011–13: US Geological Survey Scientific Investigations Report 2014–5218, 14 p.

McMahon, P., Dennehy, K., Bruce, B., Böhlke, J., Michel, R., Gurdak, J., Hurlbut, D., 2006. Storage and transit time of chemicals in thick unsaturated zones under rangeland and irrigated cropland, High Plains, United States. Water Resources Research, 42(3), 18 p.

Playa Lakes Joint Venture playa database. Pljv.org.

Rosen, M.R., 1994. The importance of groundwater in playas: A review of playa classifications and the sedimentology and hydrology of playas. Paleoclimate and basin evolution of playa systems, Geological Society of America Special Papers 289, 1-18.

Sabin, T.J., Holliday, V.T., 1995. Playas and Lunettes on the Southern High Plains: Morphometric and Spatial Relationships. Annals of the Association of American Geographers, 85(2), 286-305.

Scanlon, B.R., Goldsmith, R.S., 1997. Field study of spatial variability in unsaturated flow beneath and adjacent to playas. Water Resources Research, 33(10), 2239-2252.

Soil Survey Staff, Natural Resources Conservation Service, United States Department of Agriculture. Web Soil Survey. Available online at the following link: http://websoilsurvey.sc.egov.usda.gov/. Accessed 21 September 2018.

Tiner, R.W., 2003. Geographically isolated wetlands of the United States. Wetlands, 23(3), 494-516.

Veregin, H., 2005. Goode's World Atlas. 21st ed. Rand McNally, USA.

Wood, W.W., Osterkamp, W., 1987. Playa-lake basins on the Southern High Plains of Texas and New Mexico: Part II. A hydrologic model and mass-balance arguments for their development. Geological Society of America Bulletin, 99(2), 224-230.

Tables

Table 1. Binary chart for selection of PLSs for subset*

County	Playa - 0	Playa - 1	Lunette - 0	Lunette - 1	Included in subset**
Cheyenne	5	1	3	3	0
Clark	1	3	1	3	2
Edwards	1	0	0	1	0
Finney	3	17	12	8	6
Ford	0	2	0	2	2
Grant	0	3	2	1	1
Gray	1	7	1	7	6
Greeley	0	1	1	0	0
Haskell	1	0	0	1	0
Lane	4	13	1	16	13
Logan	0	1	1	0	0
Meade	2	1	0	3	1
Morton	1	1	1	1	1
Ness	0	1	1	0	0
Rawlins	0	1	1	0	0
Scott	6	8	4	10	6
Sherman	2	2	1	3	1
Stanton	2	3	2	3	1
Thomas	2	3	3	2	0
Wallace	2	3	4	1	0
Total	33	71	39	65	40

*There were some PLSs with values of ‘1’ could have been assigned values of ‘2’ and been interchanged and included

**PLSs included in subset had both the playa and lunette given a value of ‘1’

Table 2. Contours chosen in OS vs SS

Subset	Same in OS and SS	Larger OS	Larger SS
Playa	28	12	0
Lunette	7	32	1

Table 3. Elevation differences between OS and SS datasets

Subset	Average Elevation Difference OS – SS (all values)	Average Elevation Difference OS - SS (non-zero values)
Playa	0.31	1.04
Lunette	-0.75	-0.91

Table 4. Data results from OS, SS, OSs, and SSs Fit Ellipse – Playas

OS Playas

	Long axis angle	Long axis length	Short axis length
min	-4.22	567.42	341.73
max	34.30	3556.20	1341.26
median	13.41	1320.79	655.33
mean	15.31	1402.31	732.28
stdev	10.99	572.99	247.74

OS smoothed Playas

	Long axis angle	Long axis length	Short axis length
min	-1.02	587.57	347.68
max	35.24	3576.67	1338.90
median	13.99	1325.95	670.41
mean	15.32	1412.39	740.19
stdev	10.74	579.08	250.47

SS Playas

	Long axis angle	Long axis length	Short axis length
min	-1.08	567.42	341.73
max	34.30	3556.20	1341.26
median	12.45	1294.13	636.37
mean	14.78	1369.75	705.92
stdev	9.88	587.18	246.35

SS smoothed Playas

	Long axis angle	Long axis length	Short axis length
min	-0.84	587.57	347.68
max	35.24	3576.67	1338.90
median	13.42	1294.63	638.41
mean	14.89	1378.84	713.71
stdev	9.67	593.78	249.21

Note: Long axis angle is in degrees, long axis length is in m, and short axis length is in m

Table 5. Data results from OS, SS, OSs, and SSs ArcMap – Playas

OS Playas

	Area_m2	Area_ha	Perim_m	MBG_Width	MBG_Length	MBG_Orient
min	145714.23	14.57	2785.64	343.42	576.40	-11.4
max	2596419.96	259.64	17996.07	1295.77	3391.04	55.5
median	613001.94	61.30	5451.50	698.57	1263.74	11.1
mean	790166.05	79.02	6563.83	766.16	1406.75	14.3
stdev	540046.01	54.00	3552.47	255.21	552.40	15.0

OS smoothed Playas

	Area_m2	Area_ha	Perim_m	MBG_Width	MBG_Length	MBG_Orient
min	145609.89	14.56	2084.67	340.58	574.28	-11.3
max	2596397.81	259.64	11313.31	1292.71	3388.28	55.7
median	612986.64	61.30	3614.44	694.04	1260.57	11.0
mean	790159.28	79.02	4310.16	763.01	1403.10	14.4
stdev	540043.37	54.00	2083.12	255.21	552.18	15.0

SS Playas

	Area_m2	Area_ha	Perim_m	MBG_Width	MBG_Length	MBG_Orient
min	145714.23	14.57	2531.27	343.42	576.40	-10.0
max	2596419.96	259.64	17996.07	1295.77	3391.04	42.3
median	565089.98	56.51	4906.40	654.93	1253.58	9.0
mean	752849.79	75.28	6340.94	737.24	1368.39	12.6
stdev	544856.48	54.49	3672.56	252.66	569.84	12.6

SS smoothed Playas

	Area_m2	Area_ha	Perim_m	MBG_Width	MBG_Length	MBG_Orient
min	145609.89	14.56	2057.93	340.58	574.28	-9.9
max	2596397.81	259.64	11313.31	1292.71	3388.28	42.3
median	565079.28	56.51	3389.60	651.40	1251.28	9.1
mean	752841.20	75.28	4171.69	734.03	1364.76	12.7
stdev	544854.08	54.49	2145.27	252.63	569.49	12.6

Note: MBG_Orient column corrected by equation 90 – x to normalize to fit_ellipse results

Table 6. Data results from OS, SS, OSs, and SSs ArcMap – Lunettes

OS Lunettes

	Area_m2	Area_ha	Perim_m	MBG_Width	MBG_Length	MBG_Orient
min	29423.22	2.94	1087.13	137.87	278.51	-1.0
max	1077230.92	107.72	11503.44	967.67	2216.08	89.4
median	138018.65	13.80	2782.09	306.48	650.79	31.0
mean	199276.02	19.93	3097.12	352.41	768.86	33.7
stdev	190365.51	19.04	1870.53	166.18	389.27	19.2

OS smoothed Lunettes

	Area_m2	Area_ha	Perim_m	MBG_Width	MBG_Length	MBG_Orient
min	29431.09	2.94	710.86	134.63	274.51	-1.3
max	1077322.11	107.73	7028.15	965.26	2212.20	89.4
median	138035.55	13.80	1809.20	303.86	647.54	31.4
mean	199268.62	19.93	2056.27	349.66	765.61	33.7
stdev	190365.40	19.04	1137.07	166.05	389.37	19.3

SS Lunettes

	Area_m2	Area_ha	Perim_m	MBG_Width	MBG_Length	MBG_Orient
min	29423.22	2.94	997.31	132.14	278.51	5.0
max	666919.35	66.69	7502.61	583.11	2012.85	63.5
median	82351.20	8.24	1805.31	223.53	533.56	28.4
mean	120283.21	12.03	2145.95	251.80	634.24	30.9
stdev	113390.46	11.34	1213.72	94.44	338.88	14.0

SS smoothed Lunettes

	Area_m2	Area_ha	Perim_m	MBG_Width	MBG_Length	MBG_Orient
min	29431.09	2.94	710.86	130.33	274.51	4.8
max	666884.59	66.69	4993.60	579.72	2010.32	63.3
median	82324.35	8.23	1355.07	221.50	531.21	28.75
mean	120272.77	12.03	1565.72	249.07	631.63	31.44
stdev	113380.54	11.34	813.62	94.39	338.97	13.66

Note: MBG_Orient column corrected by equation 90 – x to normalize to fit_ellipse results

Table 7. Bowen et al., (2018) lunette database results for subset
Lunettes

	Area	Perimeter	MBG_Width	MBG_Length	MBG_Orient
min	2.44	703.66	99.72	311.00	9.70
max	80.43	5981.38	878.02	2565.06	71.50
median	14.49	1803.41	259.51	757.62	29.60
mean	18.05	1975.28	288.92	843.89	29.92
stdev	15.90	1065.78	142.04	453.49	12.20

Note: MBG_Orient column corrected by equation 90 – x to normalize to fit_ellipse results

Table 8. Differences in data values between OS, SS, OSs, and SSs ArcMap Lunettes compared to Bowen et al., (2018) lunettes

OS Lunettes

	Area_ha	Perim_m	MBG_Width	MBG_Length	MBG_Orient
min	0.50	383.47	38.15	-32.49	-10.70
max	27.29	5522.06	89.65	-348.98	17.90
median	-0.69	978.68	46.97	-106.83	1.40
mean	1.88	1121.84	63.49	-75.03	3.78
stdev	3.14	804.75	24.14	-64.22	7.00

OS smoothed Lunettes

	Area_ha	Perim_m	MBG_Width	MBG_Length	MBG_Orient
min	0.50	7.20	34.91	-36.49	-11.00
max	27.30	1046.77	87.24	-352.86	17.90
median	-0.69	5.79	44.35	-110.08	1.80
mean	1.88	80.99	60.74	-78.28	3.78
stdev	3.14	71.29	24.01	-64.12	7.10

SS Lunettes

	Area_ha	Perim_m	MBG_Width	MBG_Length	MBG_Orient
min	0.50	293.65	32.42	-32.49	-4.70
max	-13.74	1521.23	-294.91	-552.21	-8.00
median	-6.25	1.90	-35.98	-224.06	-1.20
mean	-6.02	170.67	-37.12	-209.65	0.98
stdev	-4.56	147.94	-47.60	-114.61	1.80

SS smoothed Lunettes

	Area_ha	Perim_m	MBG_Width	MBG_Length	MBG_Orient
min	0.5	7.2	30.61	-36.49	-4.9
max	-13.74	-987.78	-298.3	-554.74	-8.2
median	-6.26	-448.34	-38.01	-226.41	-0.85
mean	-6.02	-409.56	-39.85	-212.26	1.52
stdev	-4.56	-252.16	-47.65	-114.52	1.46

Note: MBG_Orient column corrected by equation 90 – x to normalize to fit_ellipse results

Table 9. Perimeter values and differences between SS Lunette, SSs Lunette, and Bowen et al., (2018) [referenced as 'Bowen']

Perimeter of Lunettes

	SS Lunette (MBG) A	SSs Lunette (MBG) B	Percent decreased when smoothed (B-A)/A	Bowen C	Difference Unsmoothed (MBG vs Bowen) (A-C)/C	Difference Smoothed (MBG vs Bowen) (B-C)/C
min	997.31	710.86	-29%	703.66	42%	1%
max	7502.61	4993.60	-33%	5981.38	25%	-17%
median	1805.31	1355.07	-25%	1803.41	0%	-25%
mean	2145.95	1565.72	-27%	1975.28	9%	-21%
stdev	1213.72	813.62	-33%	1065.78	14%	-24%

Table 10. Circular Variance of ArcMap MBG long axis orientation; tight clustering is associated with small values (results can range from 0 to 1)

Dataset	Circular Variance
OS Playa	0.0327
OSs Playa	0.0328
SS Playa	0.0232
SSs Playa	0.0233
OS Lunette	0.0533
OSs Lunette	0.0534
SS Lunette	0.0286
SSs Lunette	0.0273

Table 11. T-Tests on major axial orientation values; the p-values are higher than the alpha value, so the H_0 would fail to be rejected (indicating that there is likely no significant difference between the means of the datasets)

Assumptions
-Two-tailed
-Homoscedasticity (same variance between two different datasets)
-H_0 = No significant difference between the means of the datasets
-alpha = 0.05 [90% confidence interval, as it is a two-tailed test and alpha is divided by 2]

Datasets	p-value
OS Playa (MBG), SS Playa (MBG)	0.5924
OS Lunette (MBG), SS Lunette (MBG)	0.4554
SSs Playa (MBG), fit_ellipse	0.4156
SSs Lunette (MBG), Bowen et al., (2018) (MBG)	0.6004

Figures

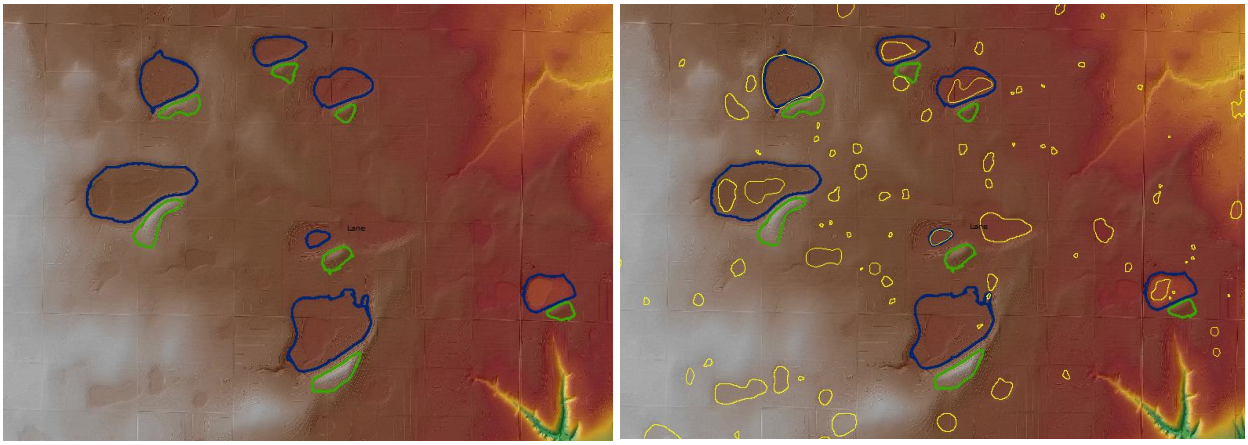

Figure 1. PLSs (playas – blue; lunettes – green) mapped during this research (left) and the PLJV wetlands mapped in the Bowen et al., (2011) research (yellow). Location: Central Lane County, Kansas

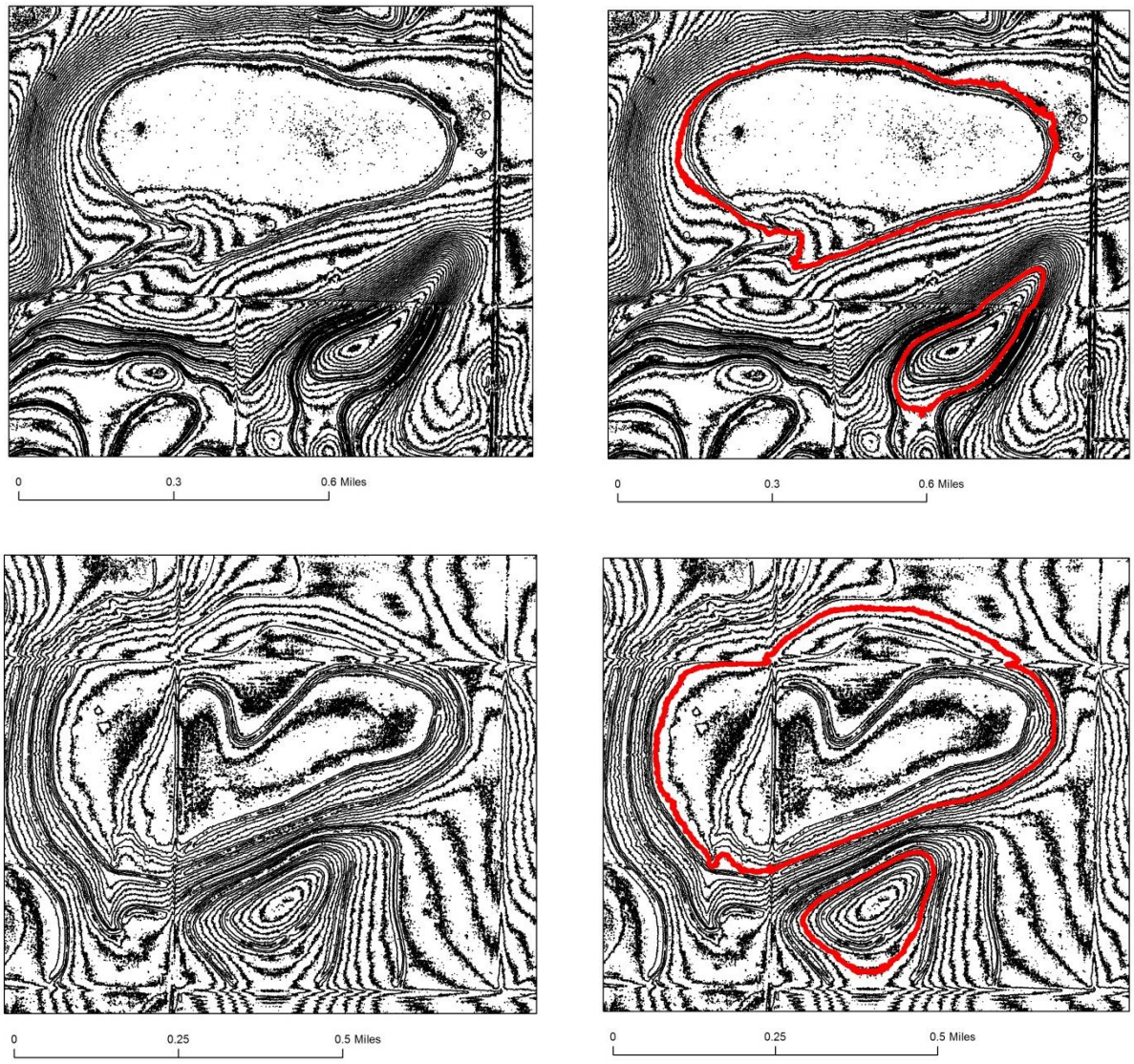

Figure 2. Contouring of two PLS examples. 0.25 m contours (black) and a mapped PLS (red, right images)

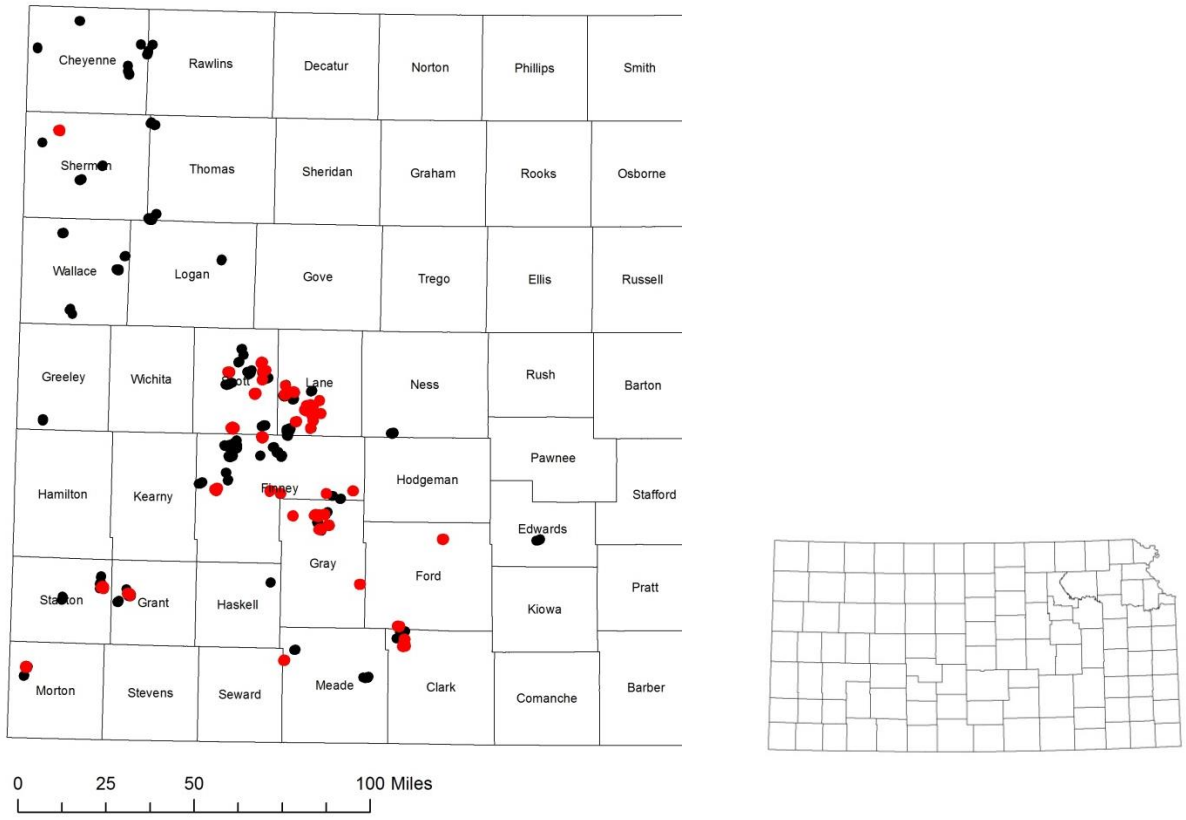

Figure 3. Distribution of lunettes in western Kansas from Bowen et al., (2018) (black and red dots) and the selected subset of PLSs (red dots).

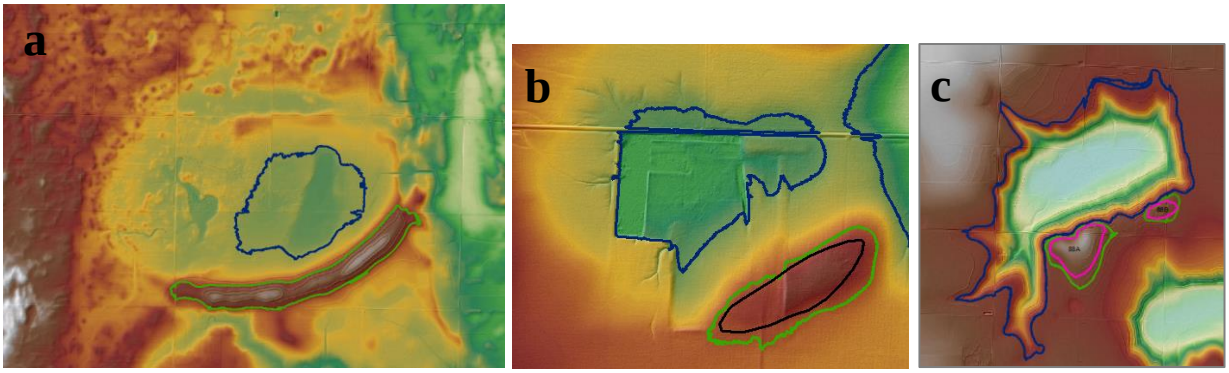

Figure 4. Examples of non-ideal playas **a.** Playa boundary (in blue) delineated was not deemed to suit the feature, so it was not included in the subset; **b.** Playa boundary was disturbed by anthropogenic influences and was no longer an ideal shape, so it was not selected for the subset; **c.** Playa boundary was noticeably affected by fluvial drainage channels, so it was not chosen for the subset.

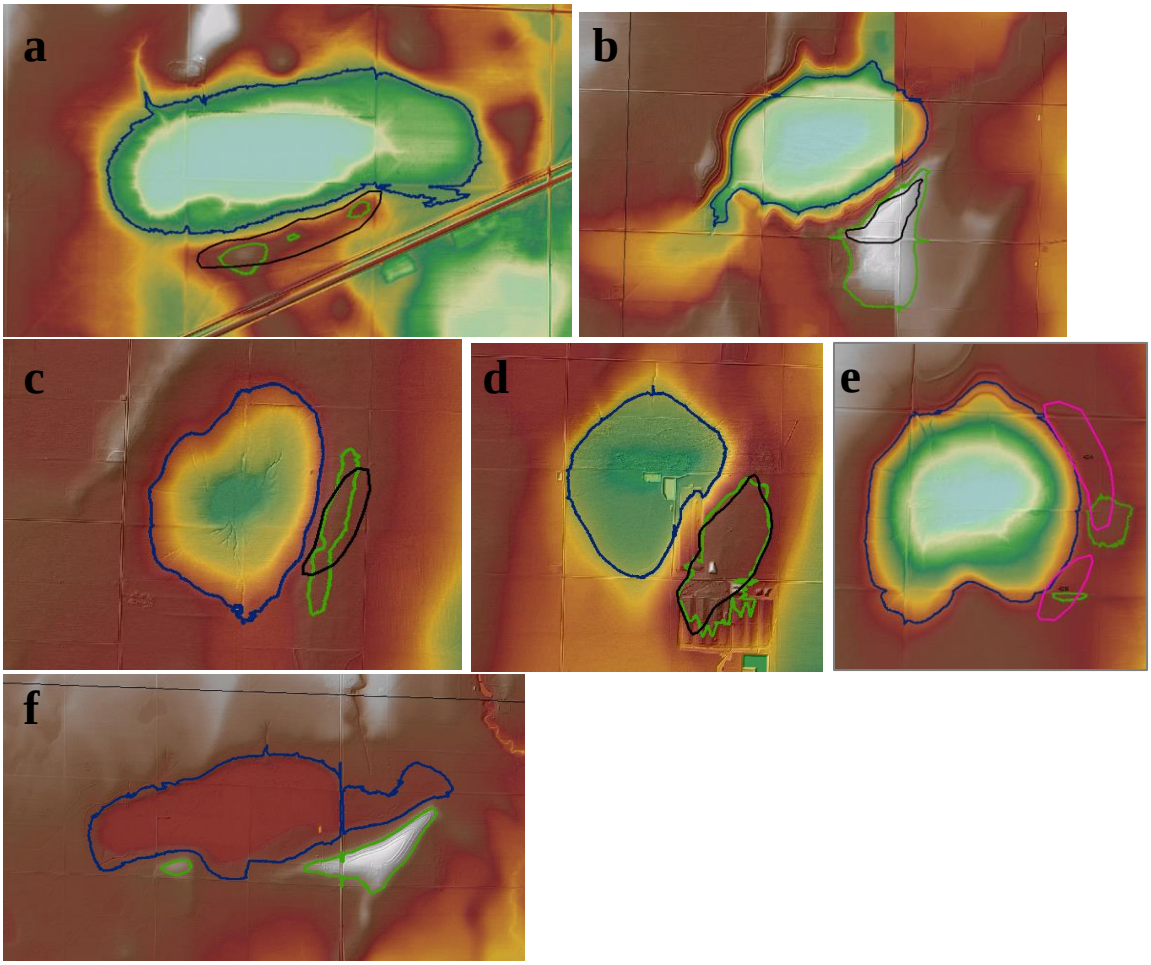

Figure 5. Examples of non-ideal lunettes **a.** Lunette was mapped as multiple high points (in green) and as a result was not chosen for the subset; **b.** Stretched lunette that was not included in the subset; **c.** Lunette was not well-defined from the surrounding landscape and was not ideal in shape or relative position to playa, so it was not included in the subset; **d.** Playa and lunette were not ideally shaped and lunette had boundary disturbances on the southern side, so it did not get added to the subset; **e.** Lunette was not easily detectable in the DEM, so this PLS did not end up being a part of the subset; **f.** PLS was a reasonable choice to include in the subset, but ultimately was not selected for the subset due to the two lunettes mapped and the off-center playa.

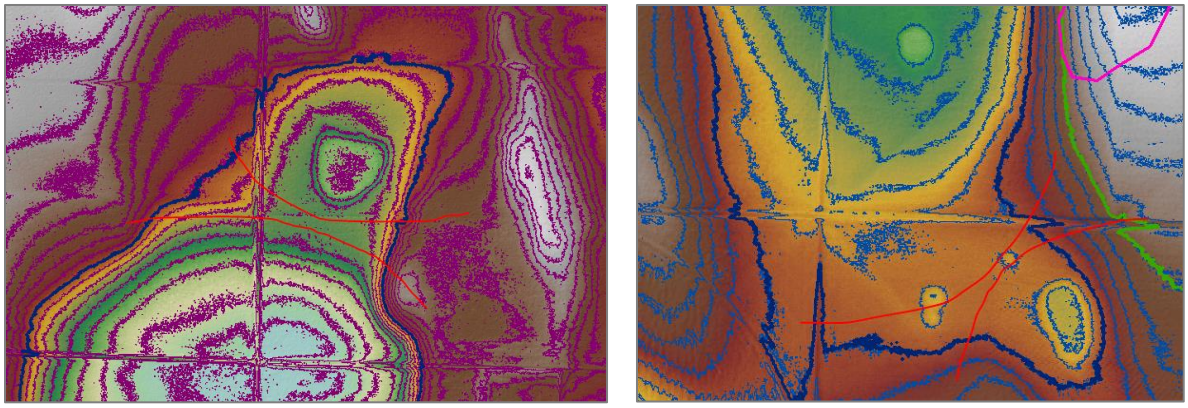

Figure 6. Examples of saddle points in playas

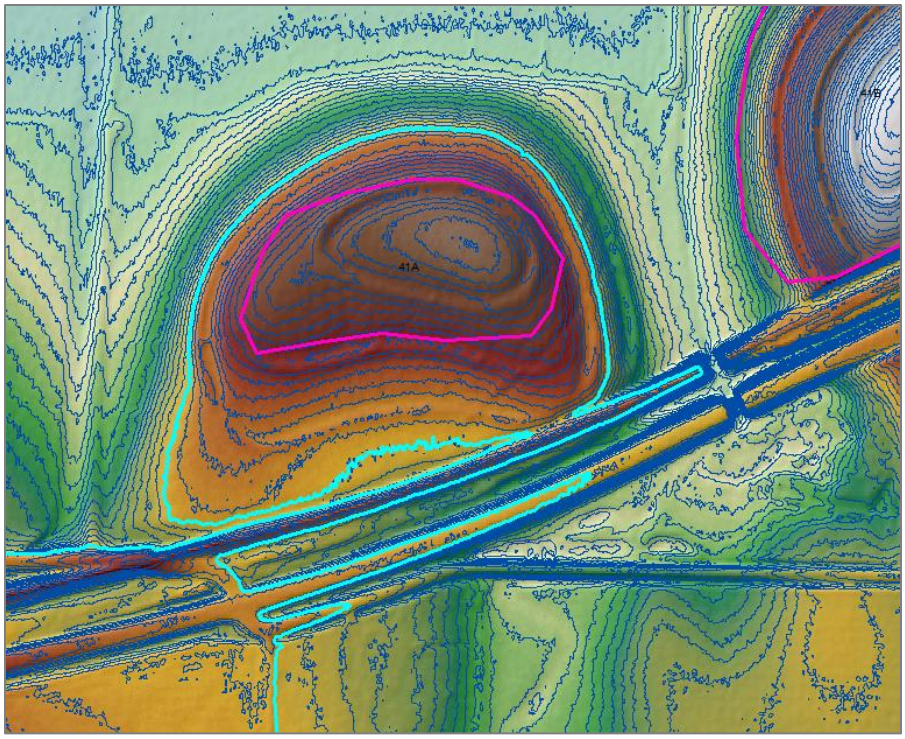

Figure 7. A road disturbance on the edge of the lunette boundary

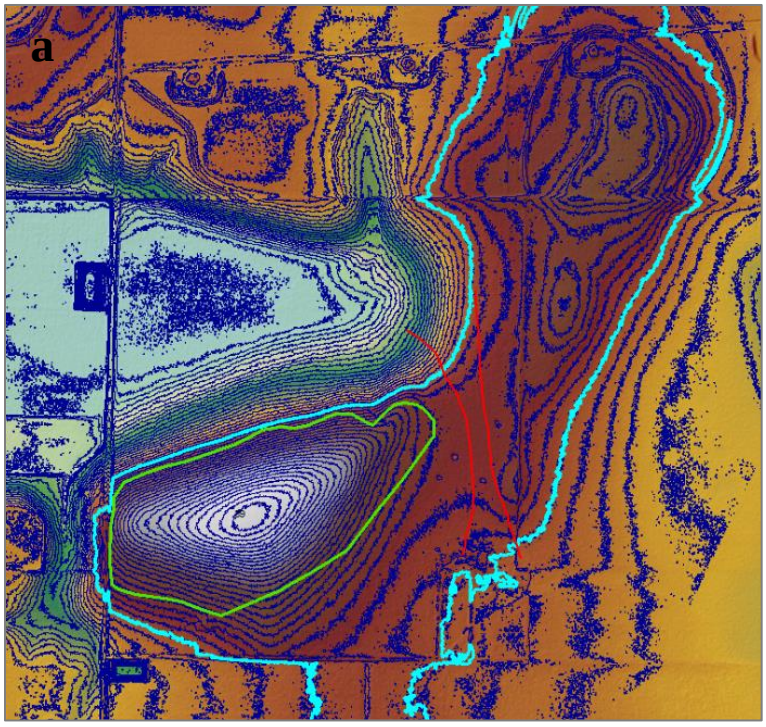

Figure 8. The largest closed contour (light blue) included an adjacent topographic high, so the saddle point (in red) was used to choose a smaller boundary

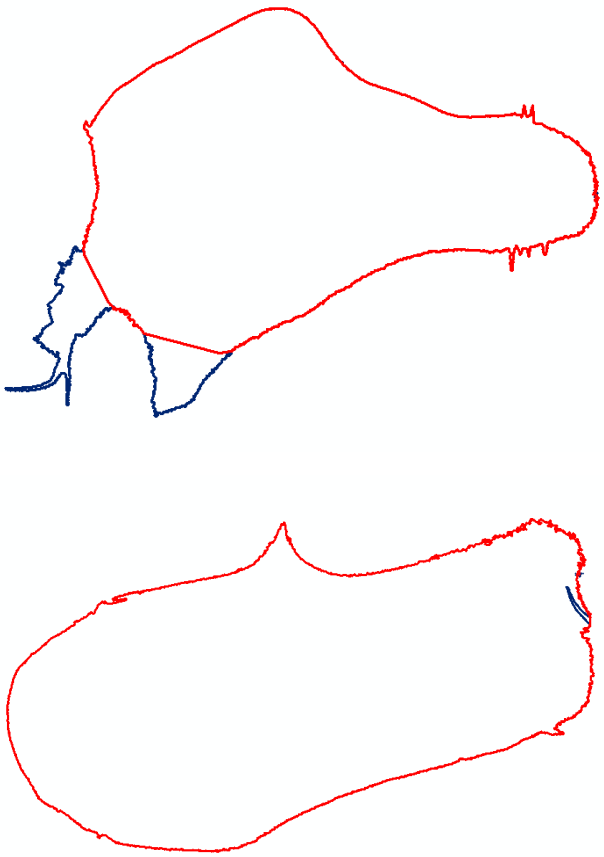

Figure 9. Fluvial channels (dark blue) were removed from the playa boundary (red) to create less noise in ellipse fitting results

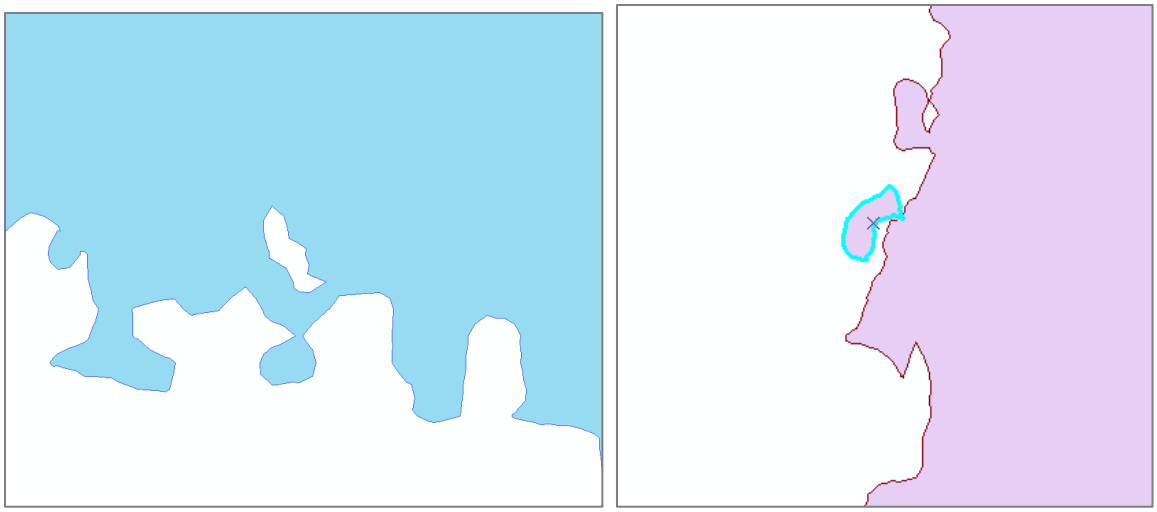

Figure 10. Converting polylines to polygons in ArcMap 10.x unintentionally created small artifacts that needed to be removed

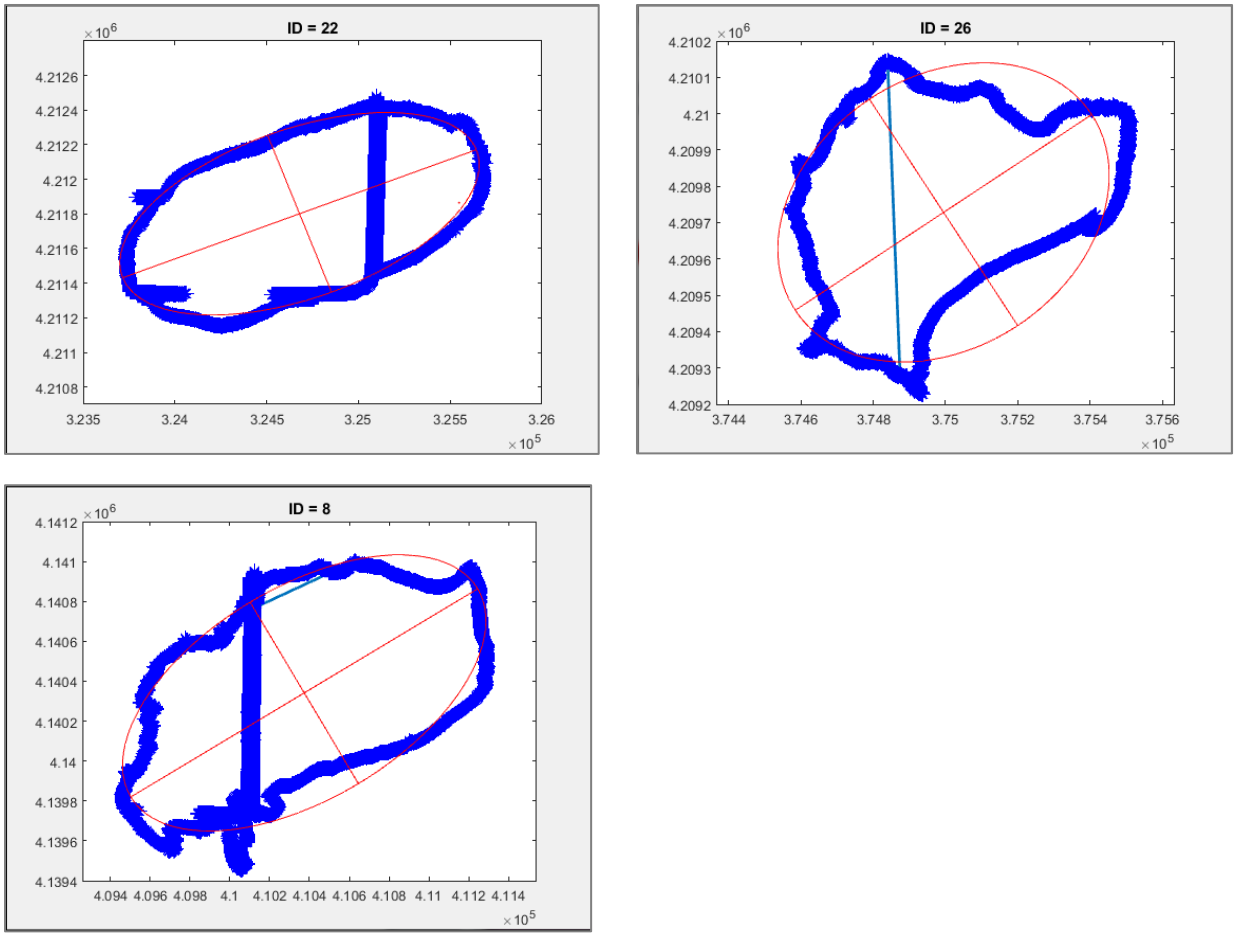

Figure 11. Examples of playas with multiple polygons (blue) fit to ellipses (red) using Matlab code fit_ellipse

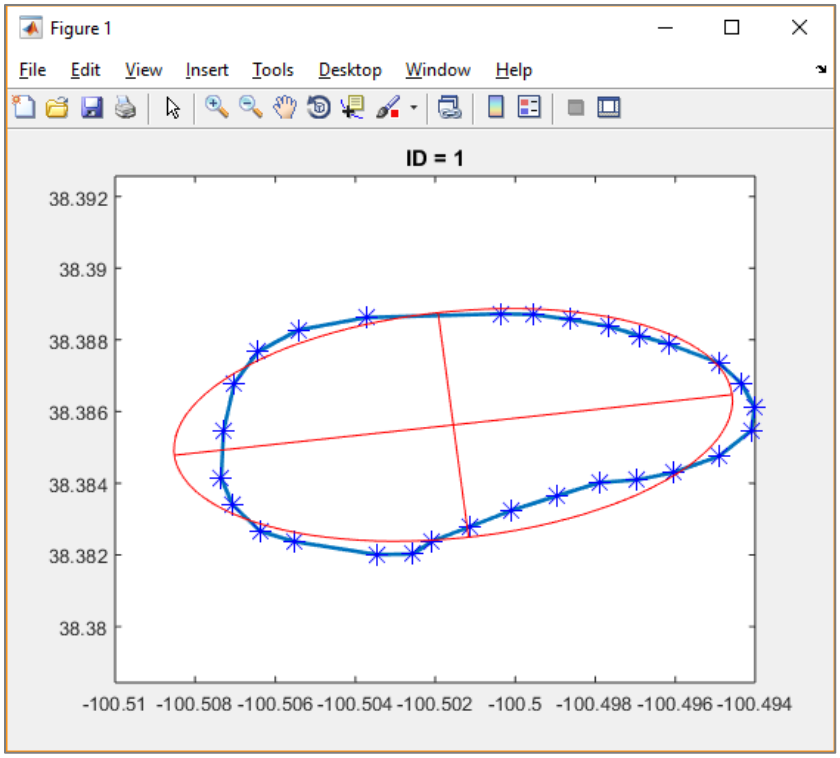

Figure 12. Playa basin fit to an ellipse using fit_ellipse code. Image generated in MATLAB

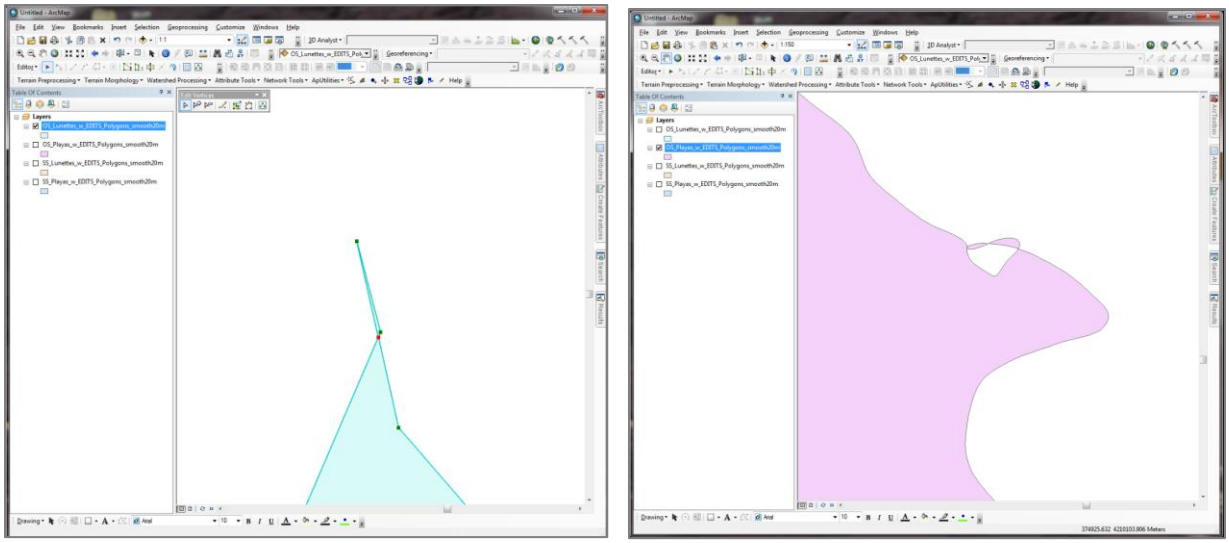

Figure 13. Topology errors that needed to be corrected when the smoothing tool was run in ArcMap 10.x

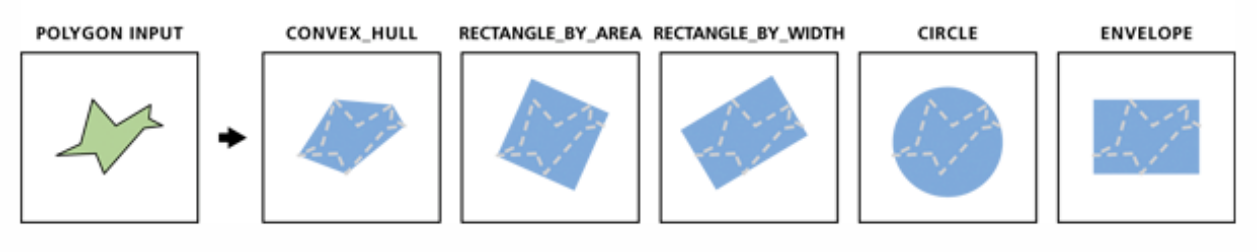

Figure 14. Polygon output options from ArcMap 10.x Minimum Bounding Geometry tool polygon output options (ESRI - MBG)

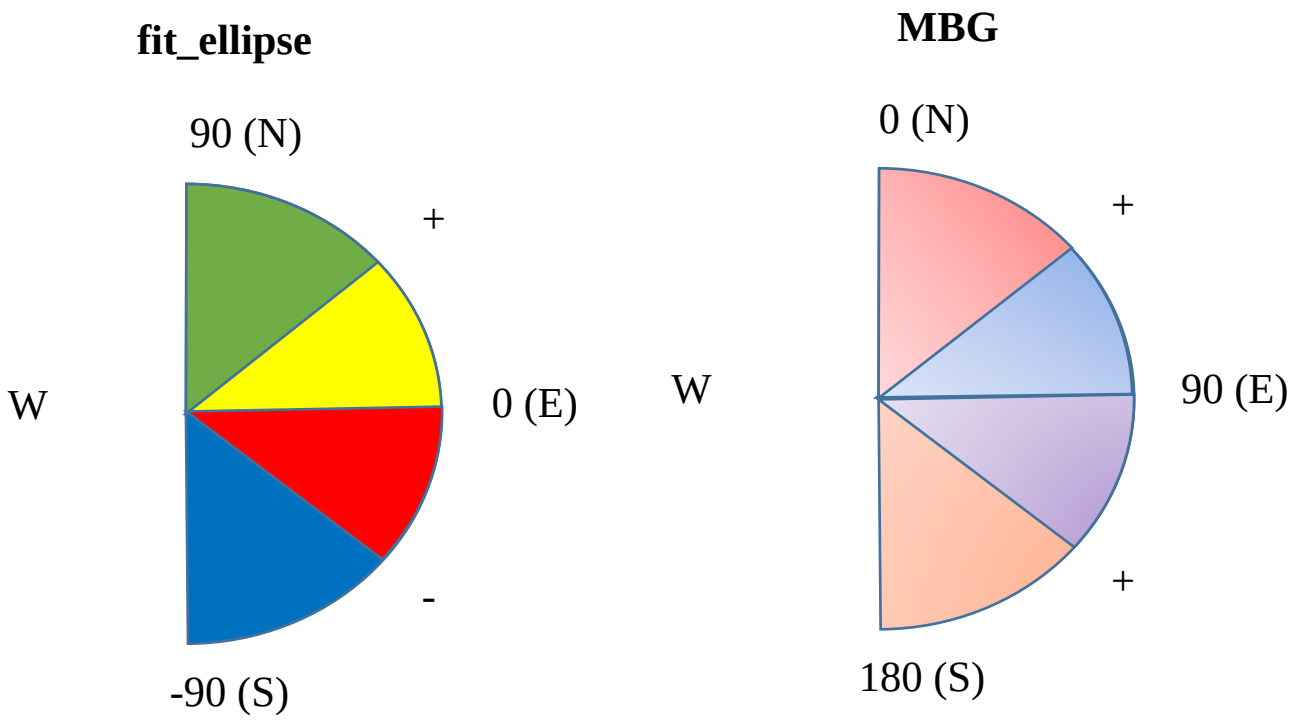

Figure 15. Charts of the angles used to describe ellipse angles. The fit_ellipse orientation scale was used as a default and the MBG orientations were converted to match using the equation: 90 – x

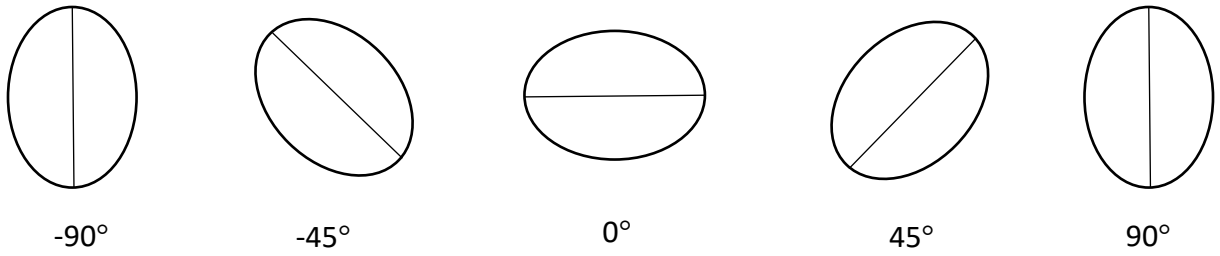

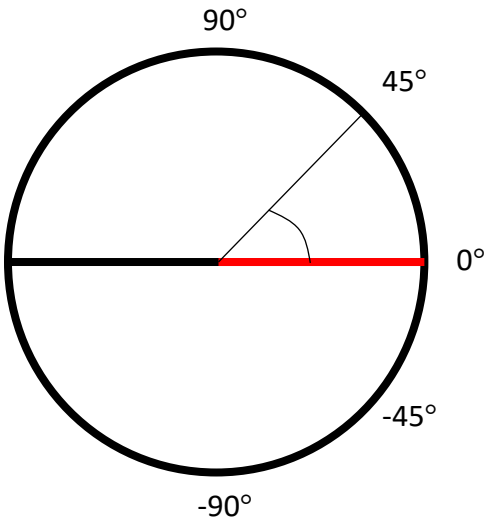

Figure 16. Playa major axial angles from a reference point, 0° (horizontal)

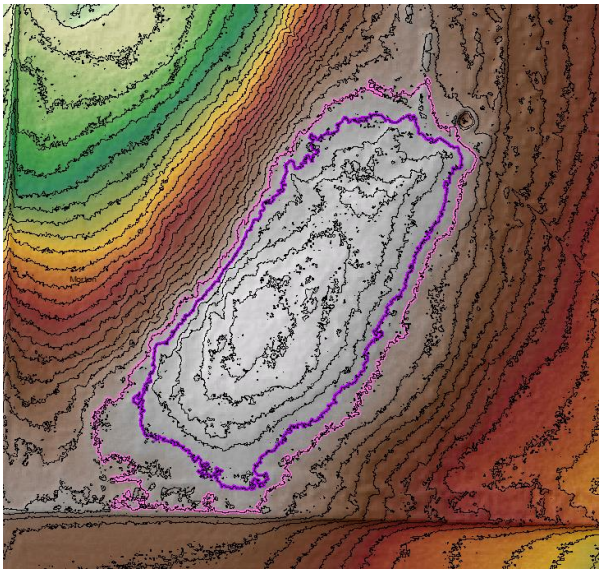

Figure 17. Example where a larger contour was chosen for SS (pink); OS in purple, contours in black

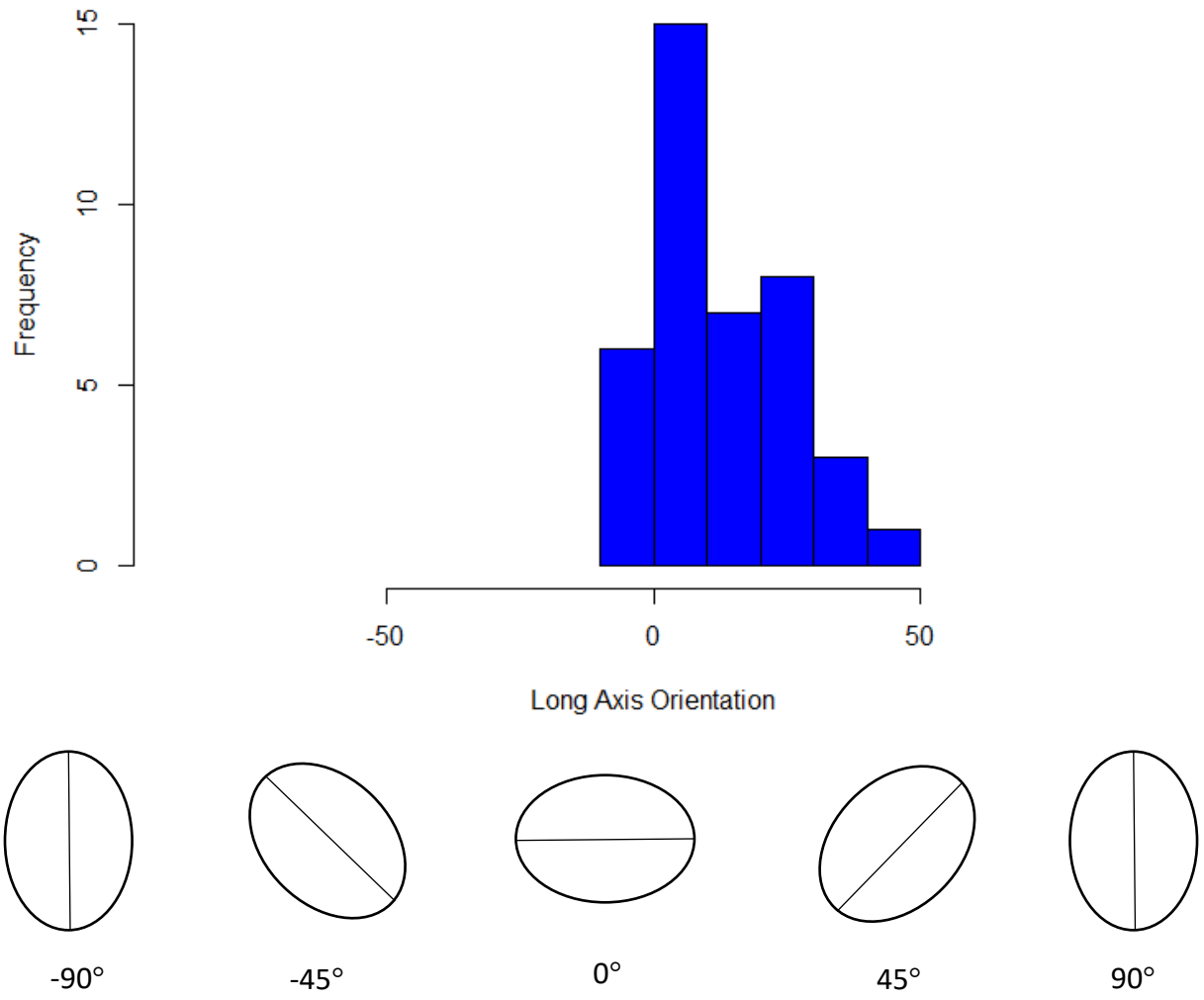

Figure 18. Playa MBG SS long axis orientation (in degrees)

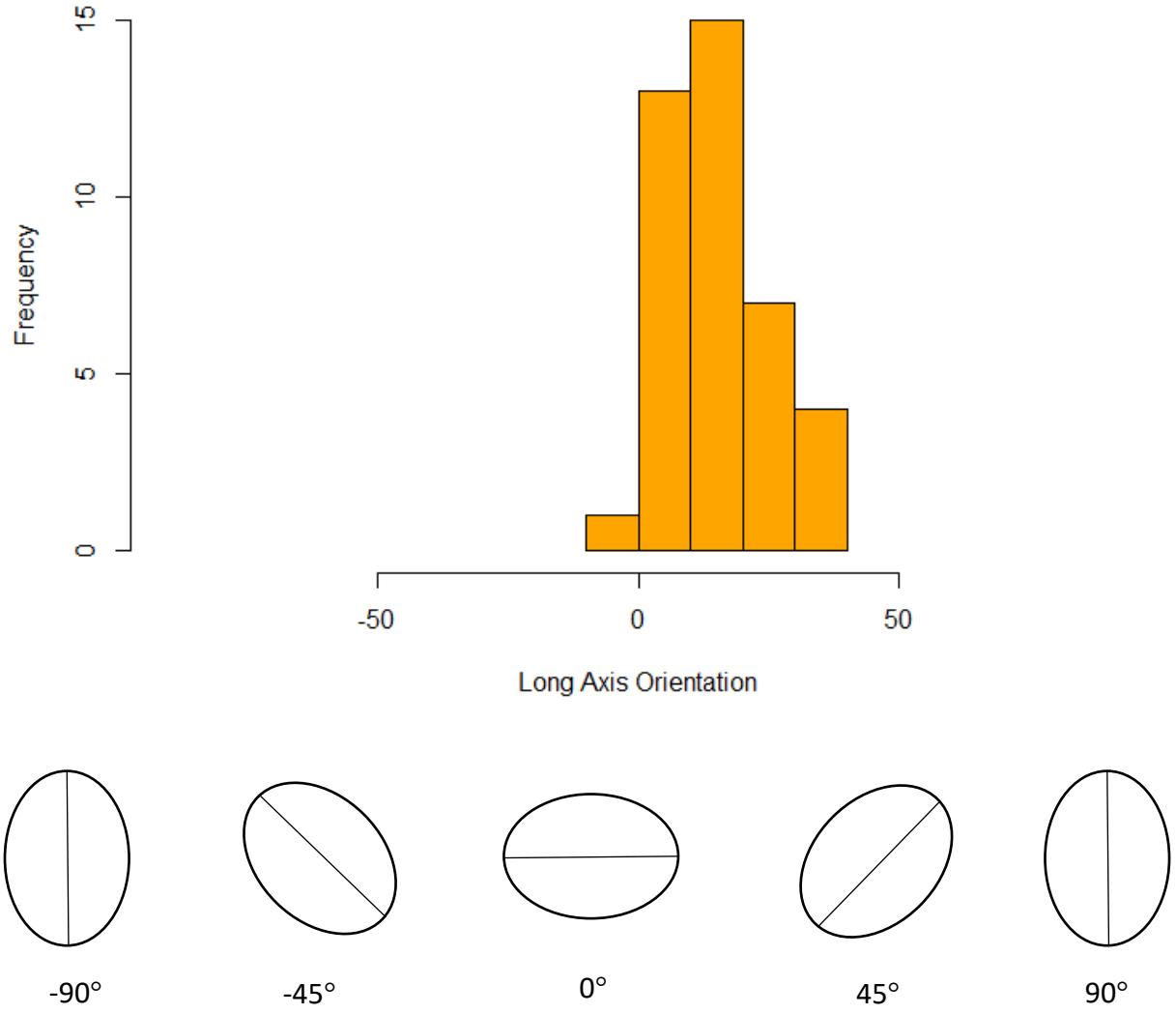

Figure 19. Playa SS fit_ellipse long axis orientation (in degrees)

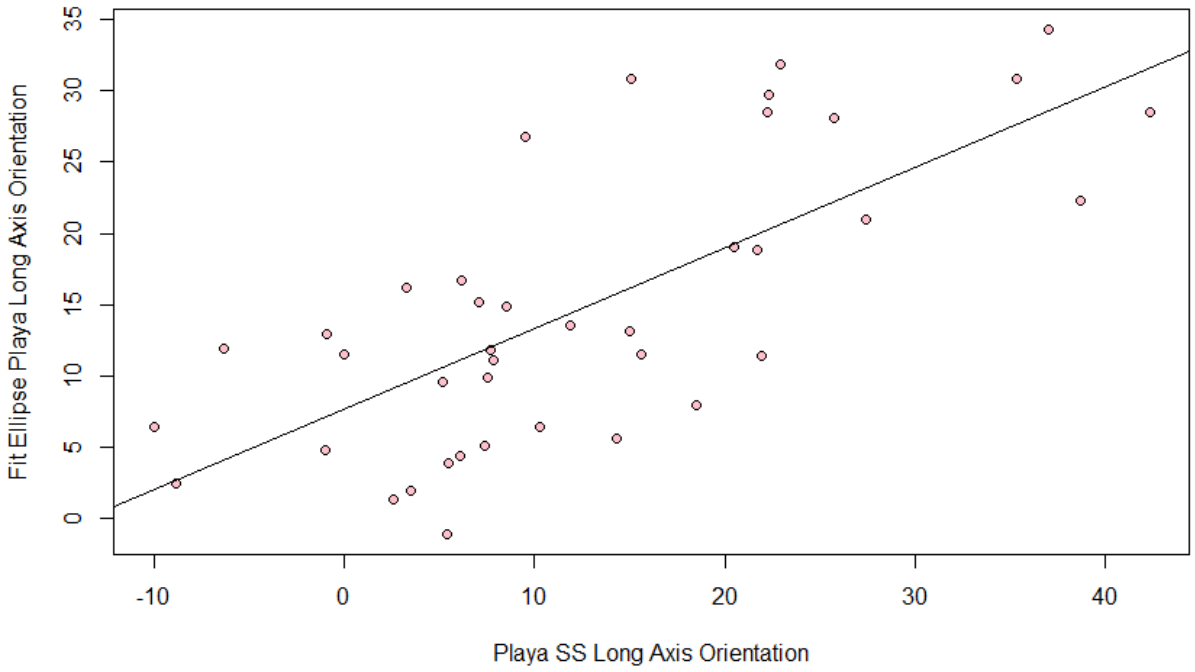

Correlation: 0.7210905

Figure 20. Playa long axis orientation – fit_ellipse SS vs MBG SS

Note: A best fit line was used in this plot

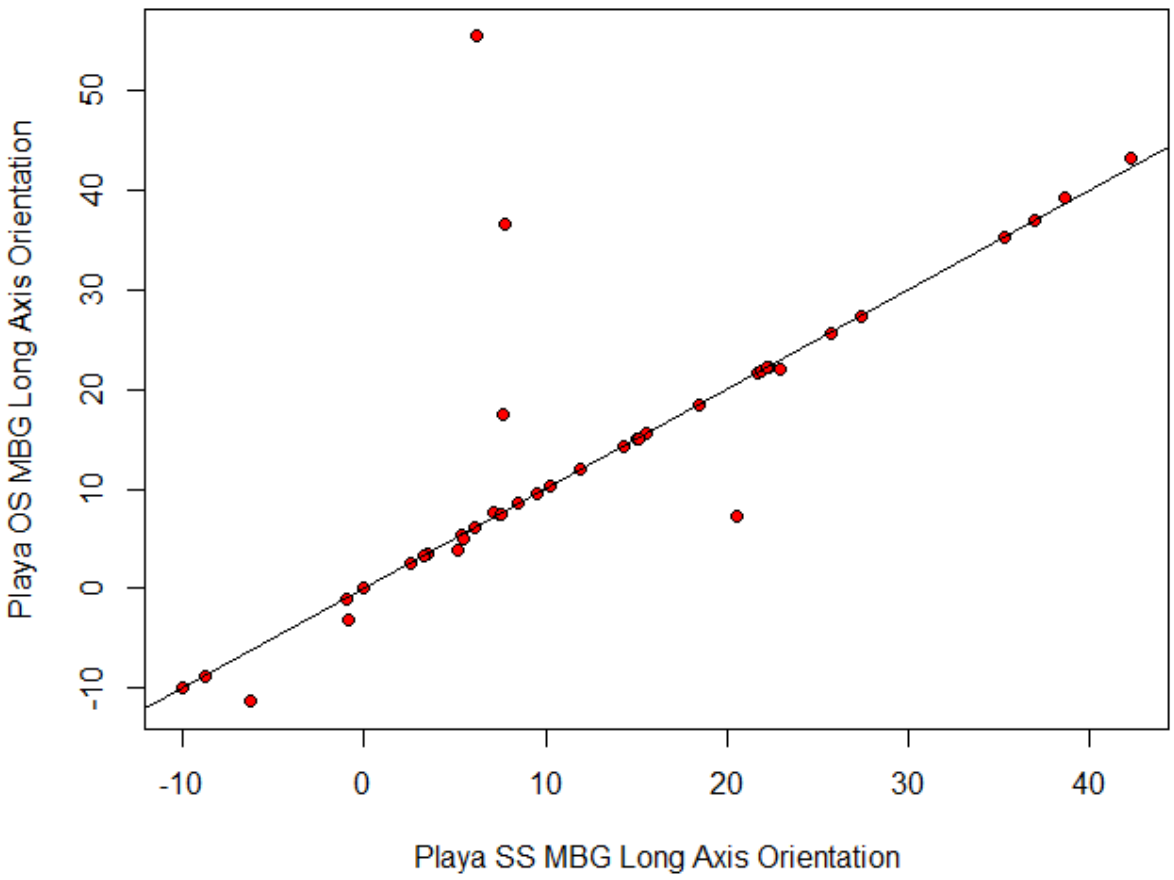

Correlation: 0.7802999

Figure 21. Playa OS vs SS MBG – long axis orientation

Note: A one-to-one line was used in this plot

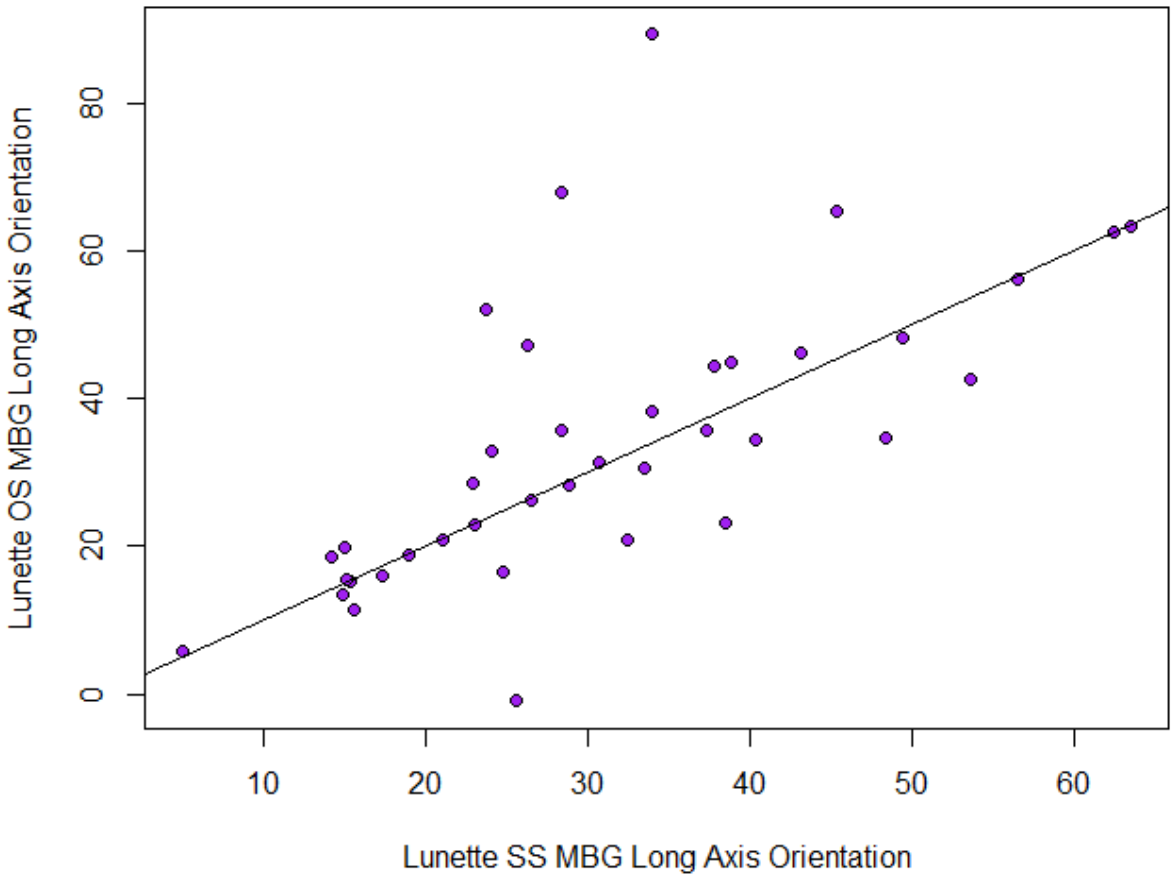

Correlation: 0.6778627

Figure 22. Lunette OS MBG long axis orientation vs lunette SS MBG long axis orientation

Note: A one-to-one line was used in this plot

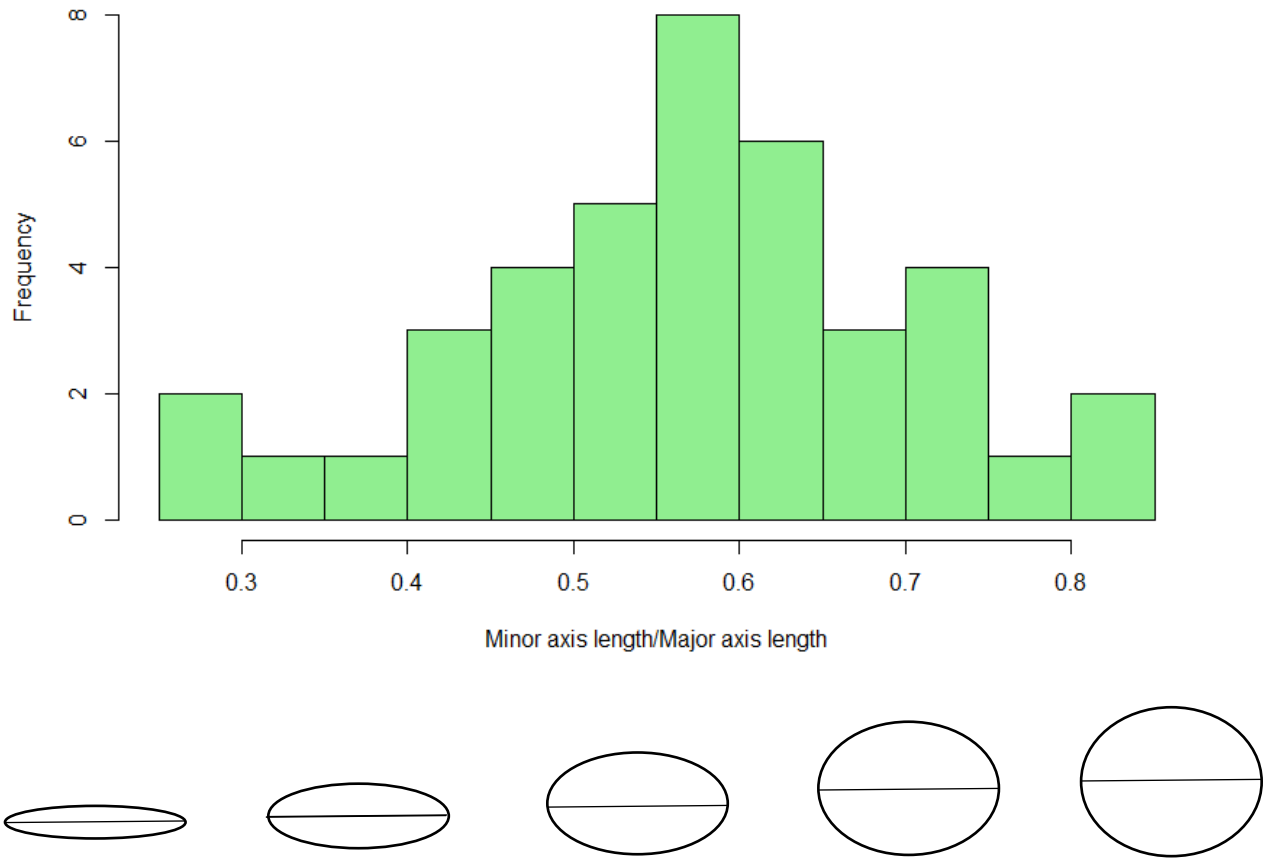

Figure 23. Playa MBG SS minor axis length divided by major axis length

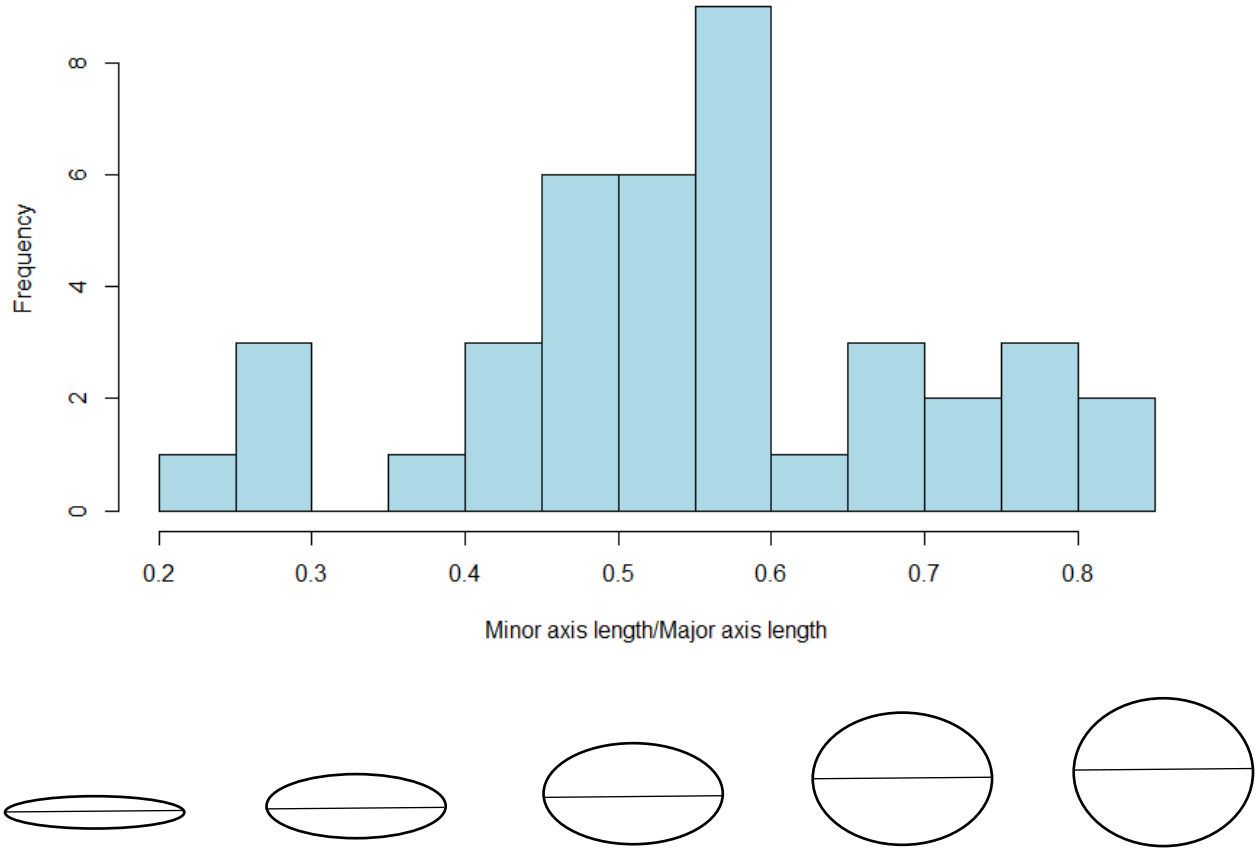

Figure 24. Playa fit_ellipse SS minor axis length divided by major axis length

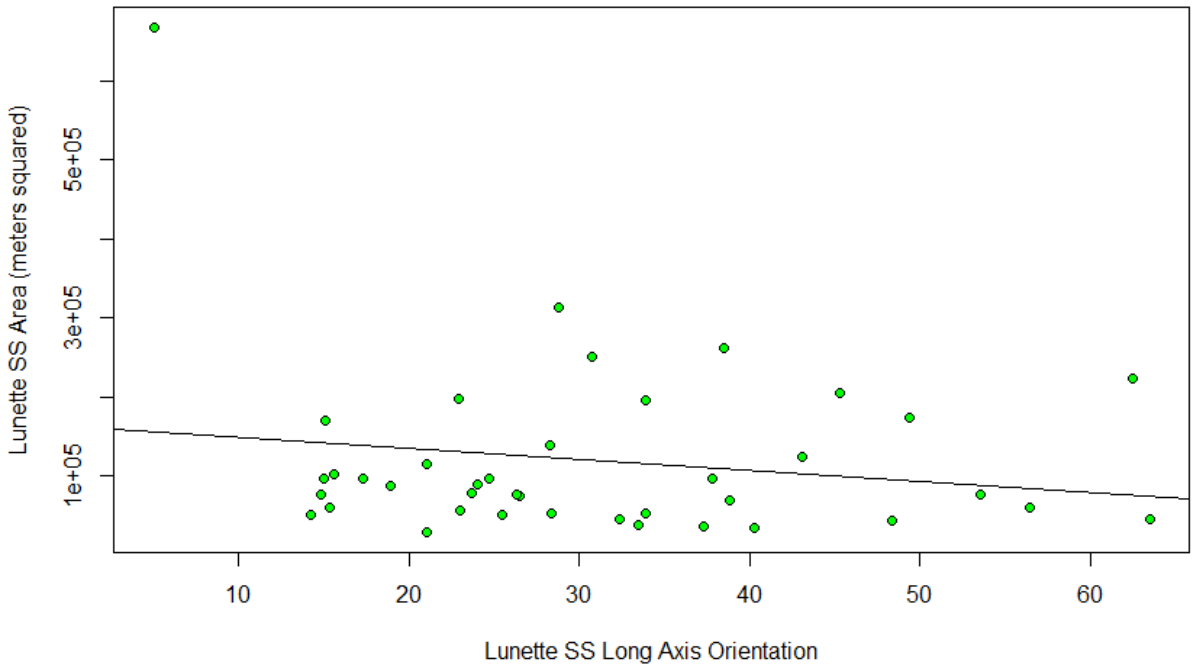

Correlation: -0.1723591

Figure 25. Lunette MBG SS – area vs long axis orientation

Note: A best fit line was used in this plot

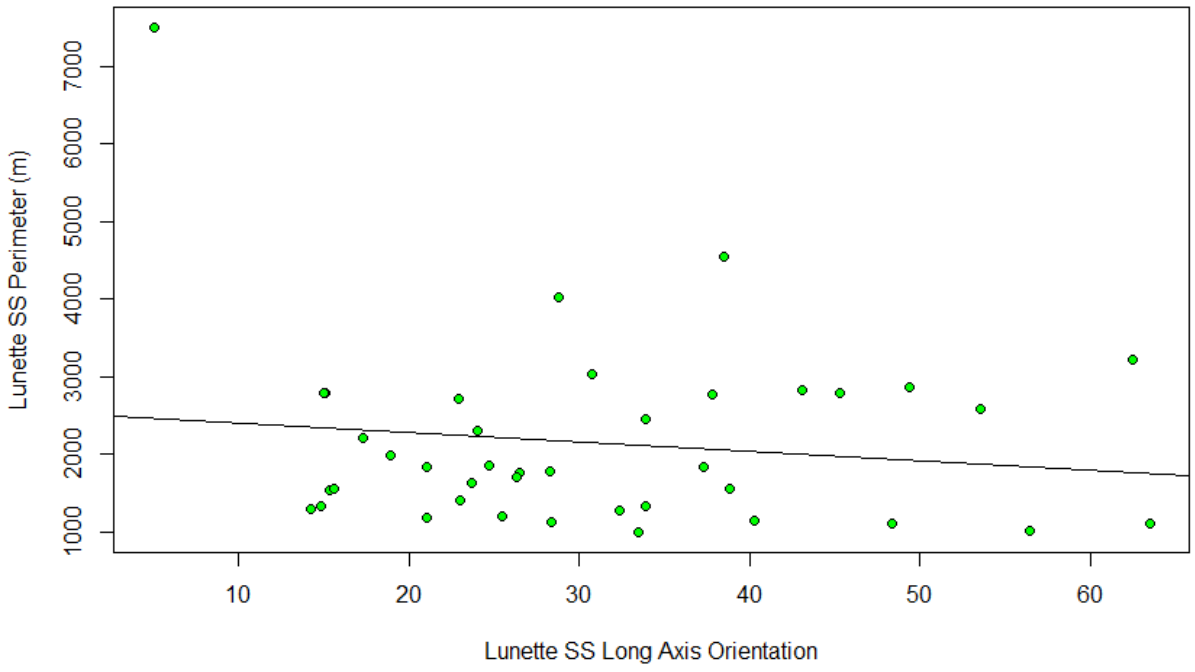

Correlation: -0.1382203

Figure 26. Lunette MBG SS – perimeter vs long axis orientation

Note: A best fit line was used in this plot

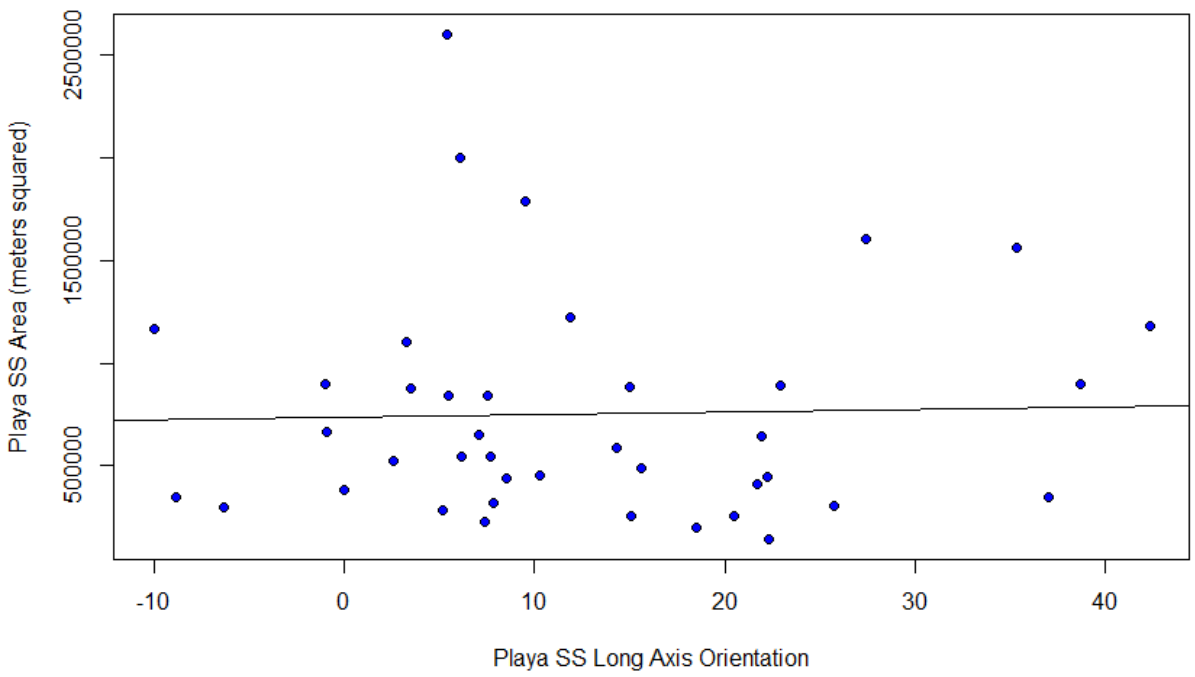

Correlation: 0.0290722

Figure 27. Playa MBG SS –area vs long axis orientation

Note: A best fit line was used in this plot

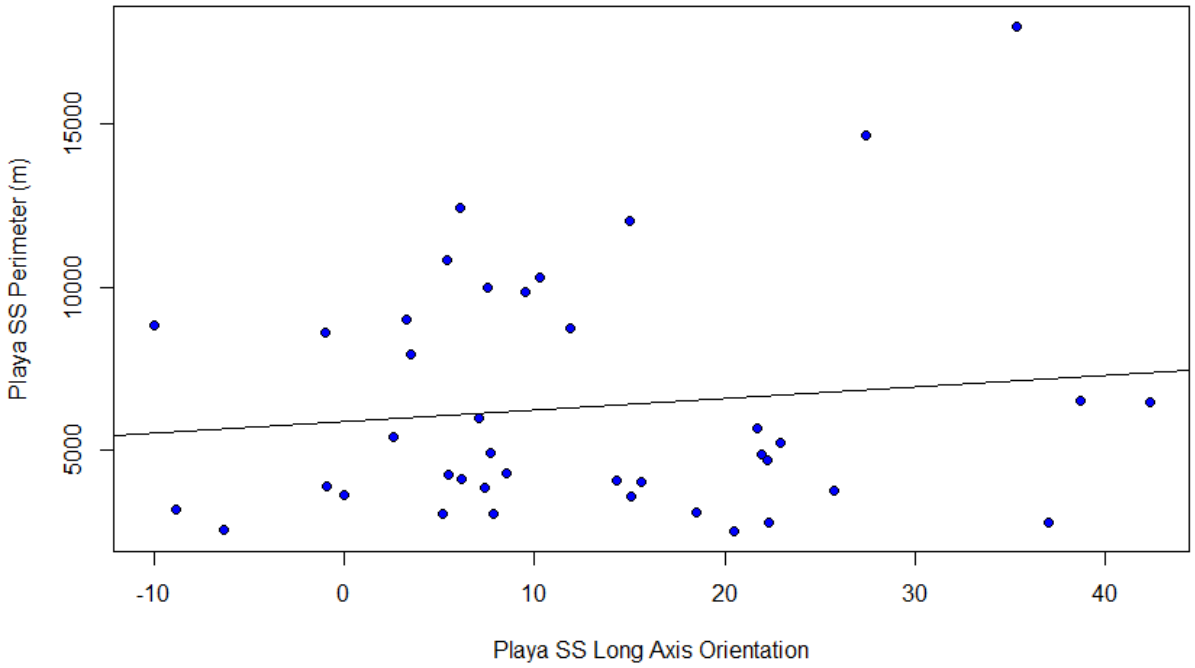

Correlation: 0.1207883

Figure 28. Playa MBG SS – perimeter vs long axis orientation

Note: A best fit line was used in this plot

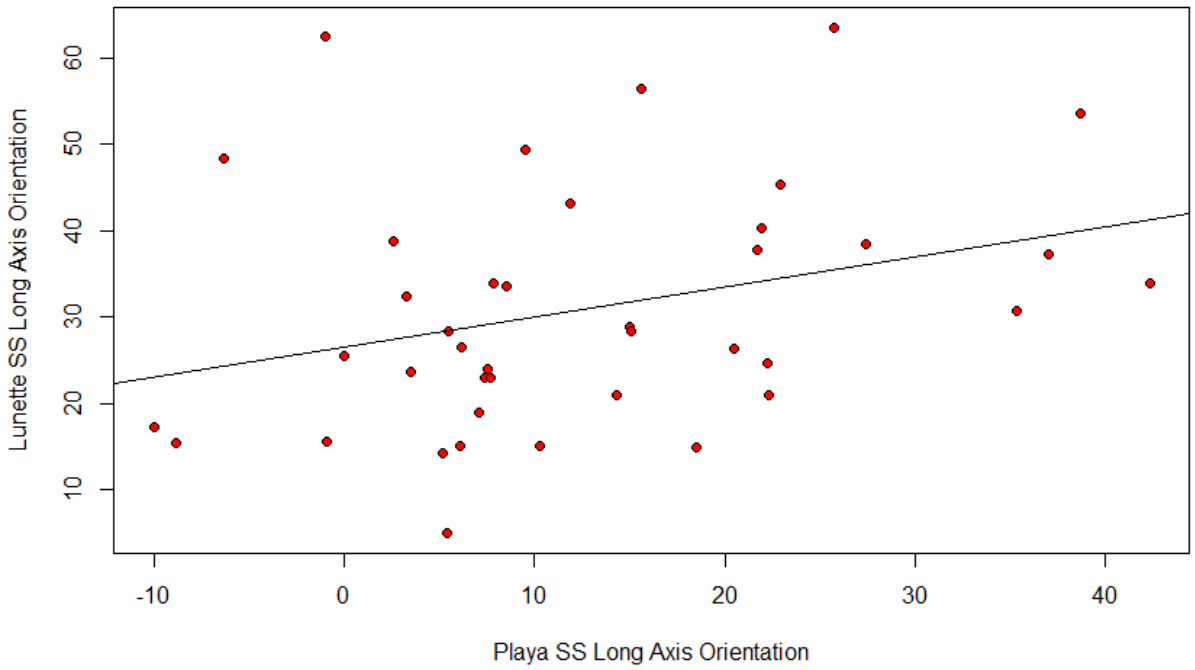

Correlation: 0.3130903

Figure 29. Lunette SS MBG long axis orientation vs playa SS MBG long axis orientation

Note: A best fit line was used in this plot

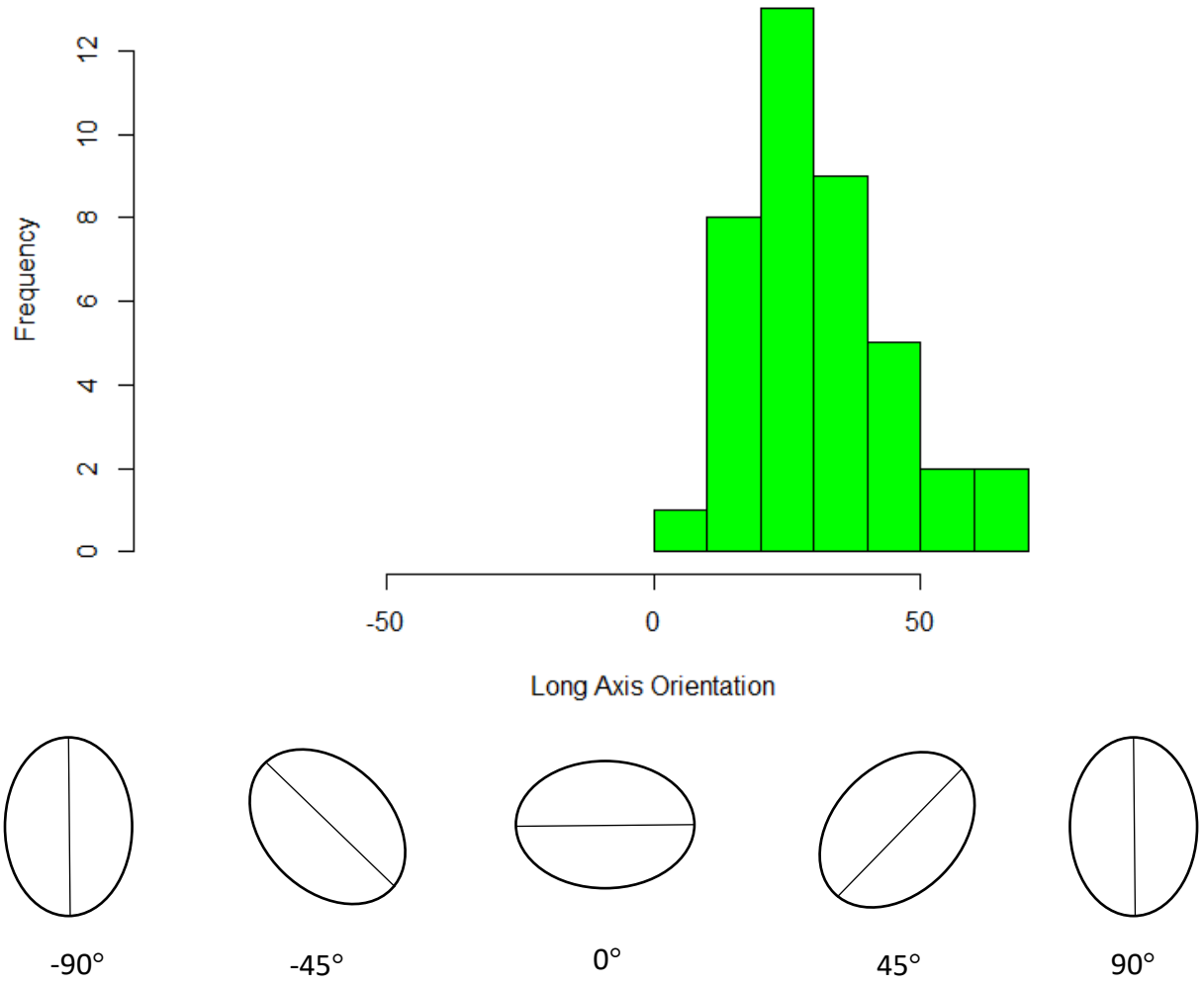

Figure 30. Lunette MBG SS long axis orientation (in degrees)

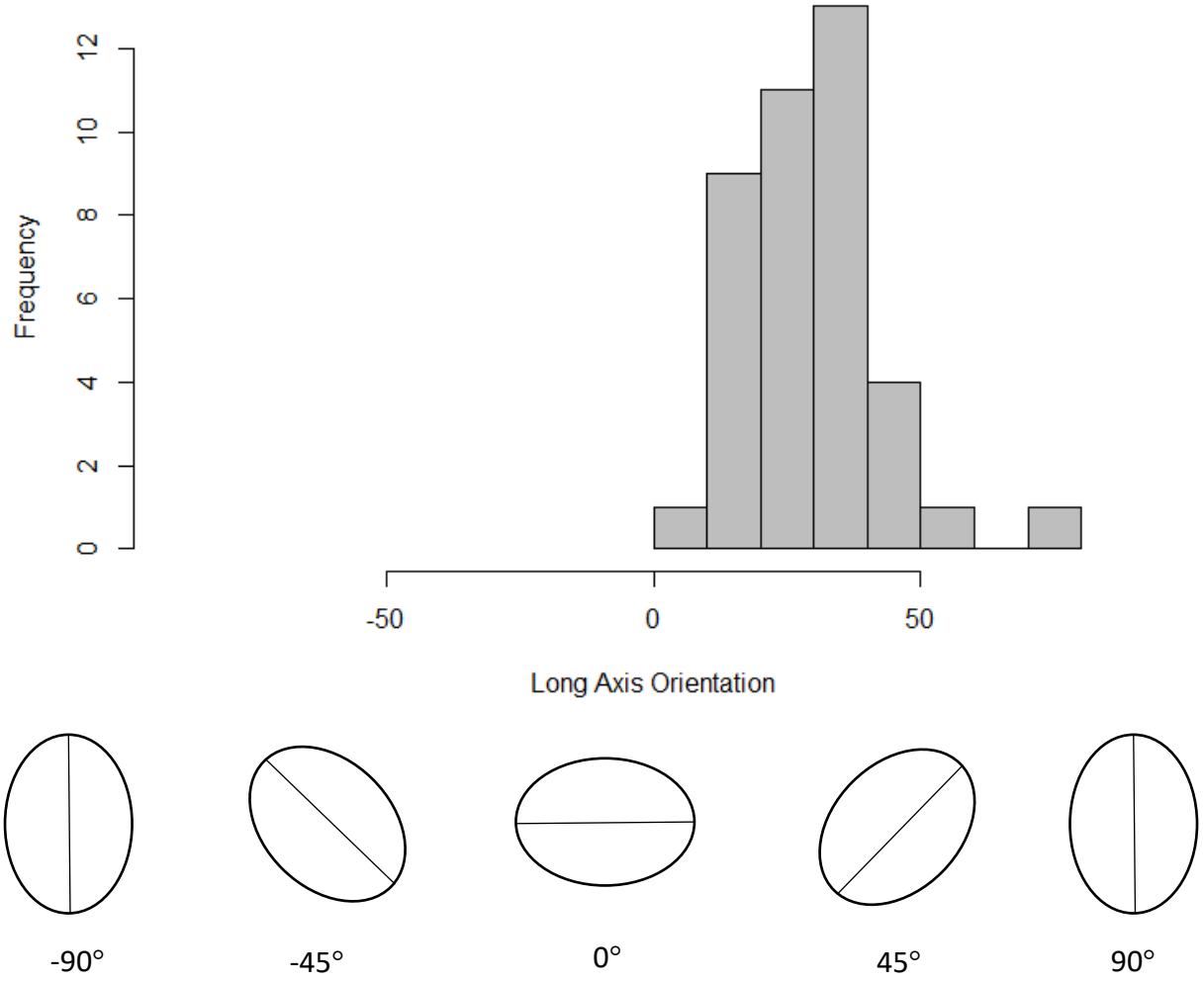

Figure 31. Bowen et al., (2018) MBG long axis orientation for subset of 40

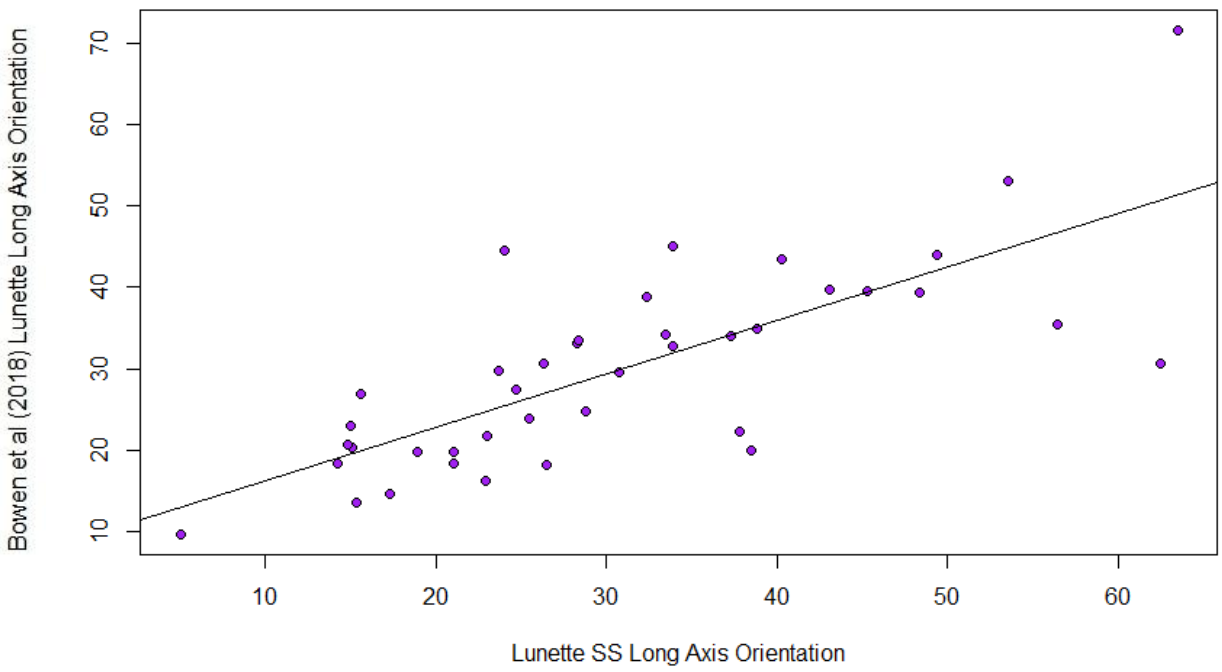

Correlation: 0.7527673

Figure 32. Subset of Bowen et al., (2018) vs MBG SS lunette long axis orientation

Note: A best fit line was used in this plot

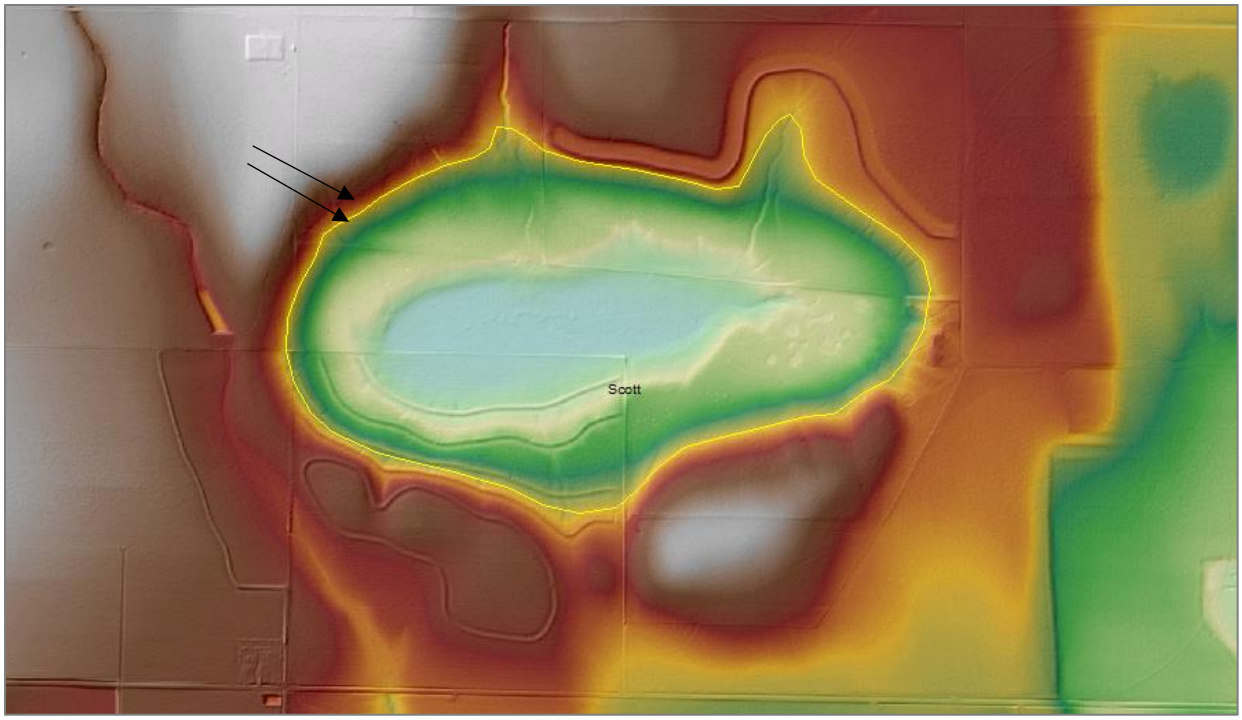

Figure 33. Subjectivities encountered at the beginning of the research included minimizing the bias as to how to define the feature's boundaries; two examples of potential boundaries indicated by black arrows

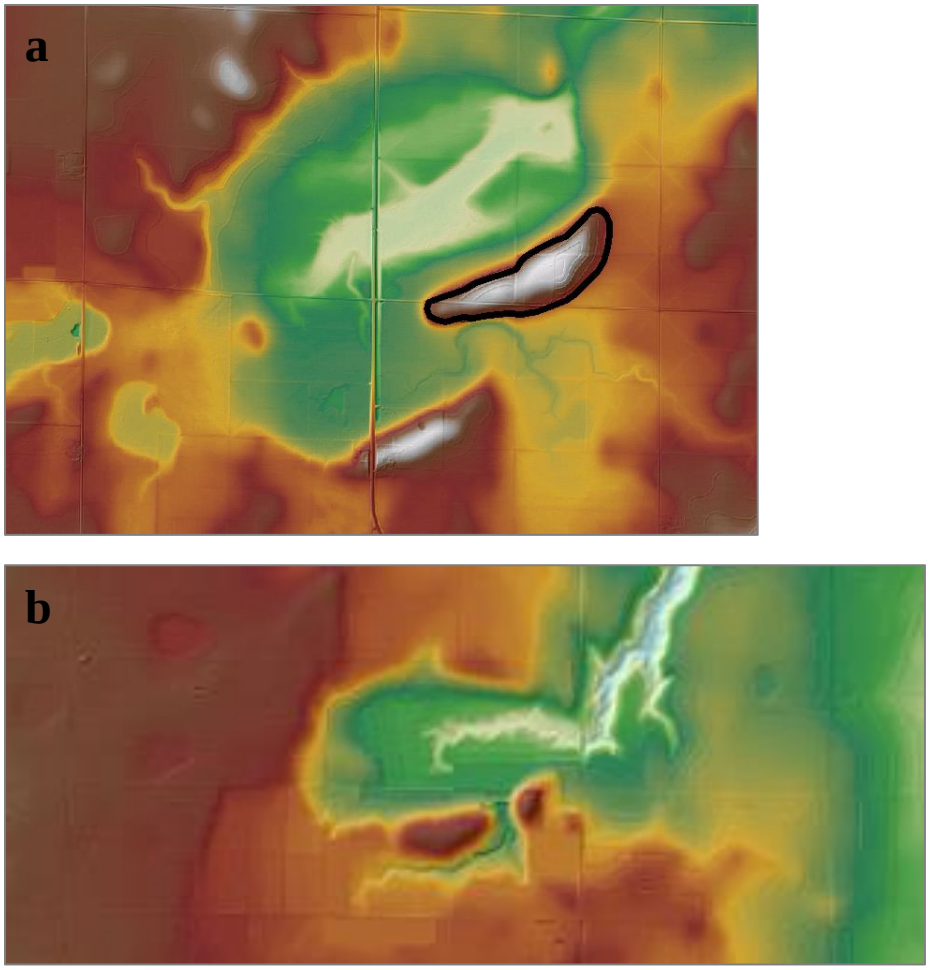

Figure 34. Using high-resolution LiDAR has the potential to yield unmapped lunettes **a.** An unmapped lunette near playa with PID 8, below left of Bowen et al., (2018) lunette outlined in black; **b.** Lane County, Kansas – 38.427° N, 100.475° W. This appears to be a PLS due to the shape of the depression/rise

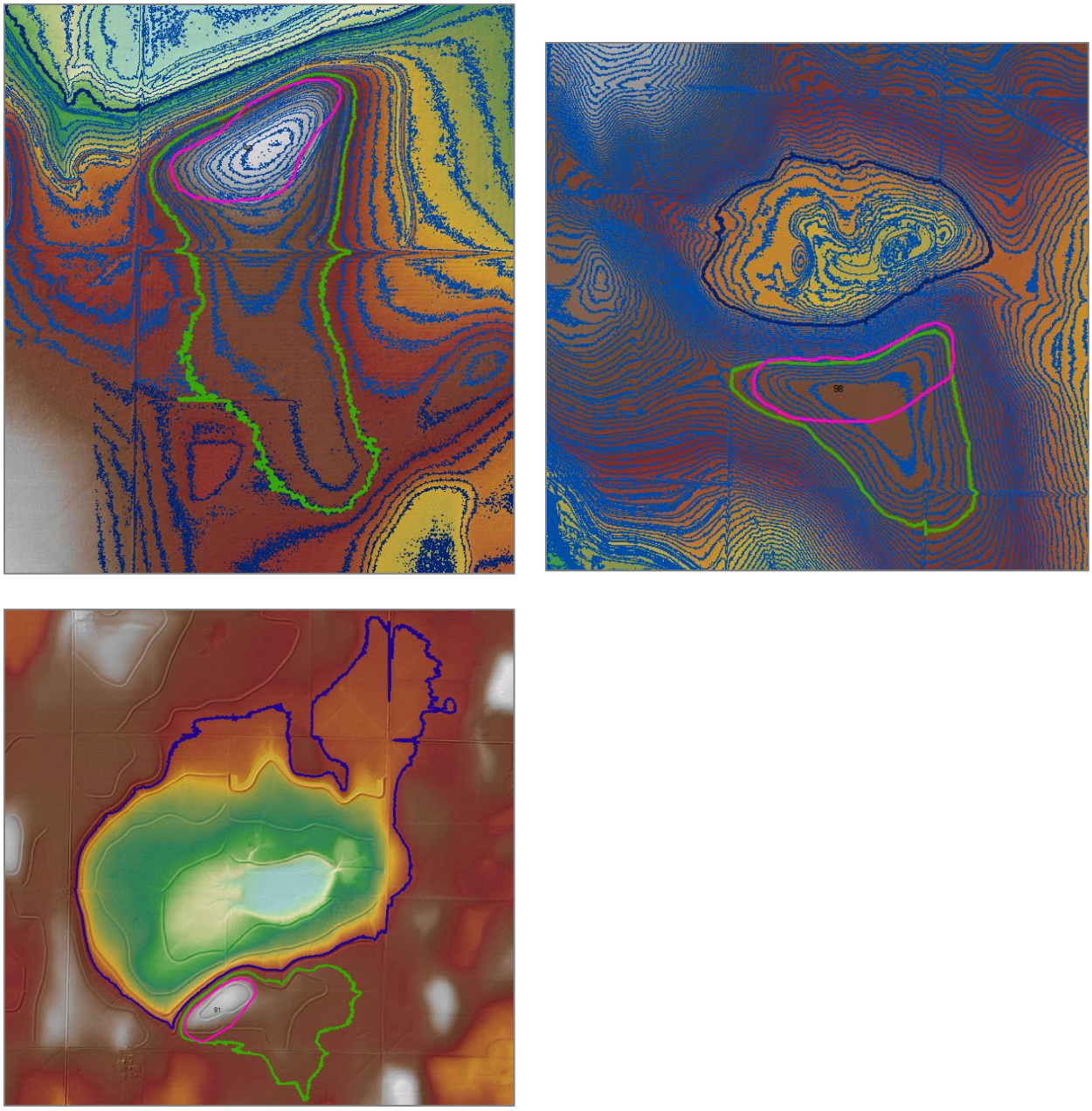

Figure 35. Three examples of stretched lunettes

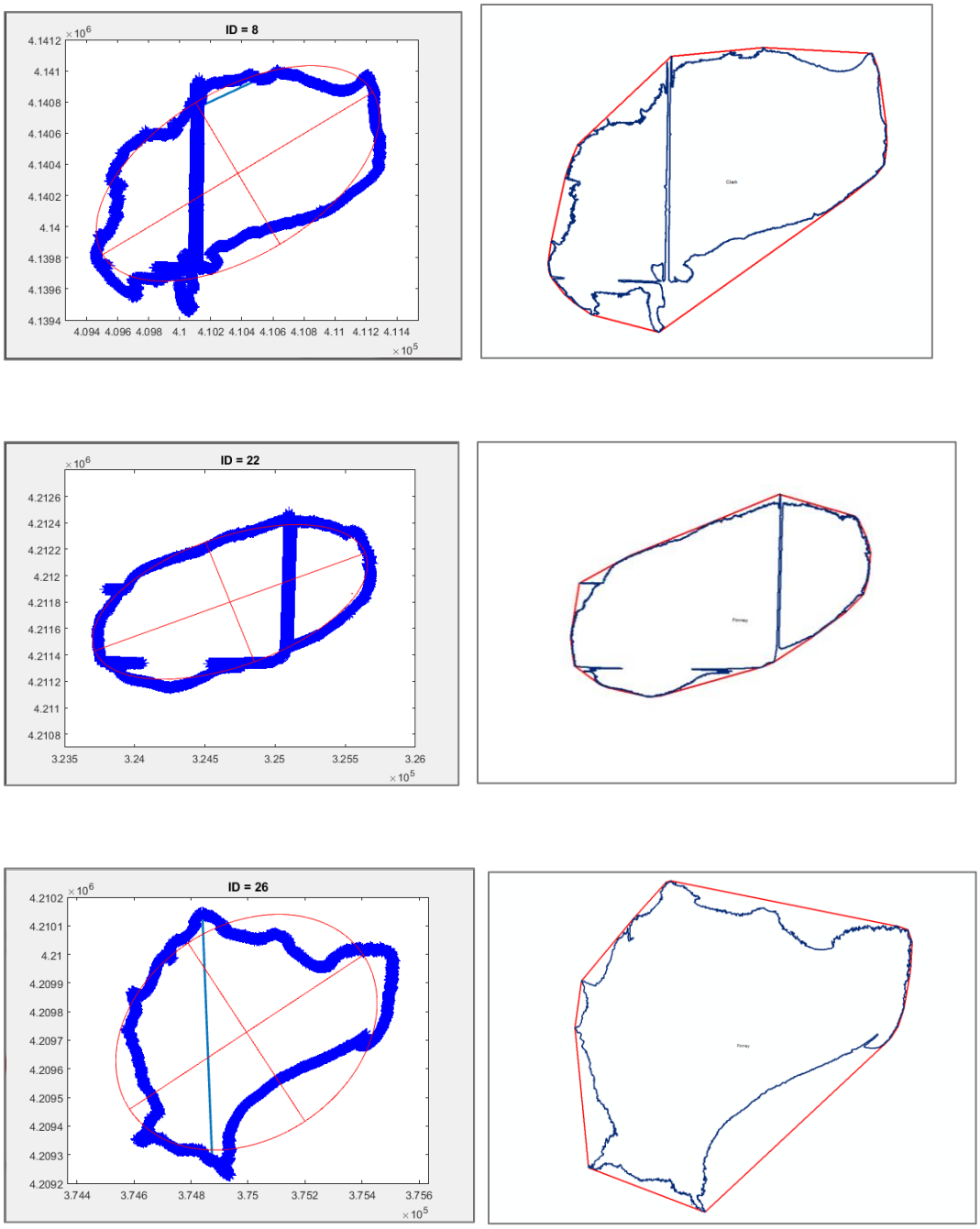

Figure 36. Examples of fit_ellipse ellipses (left) versus MBG convex hull around playas (right)

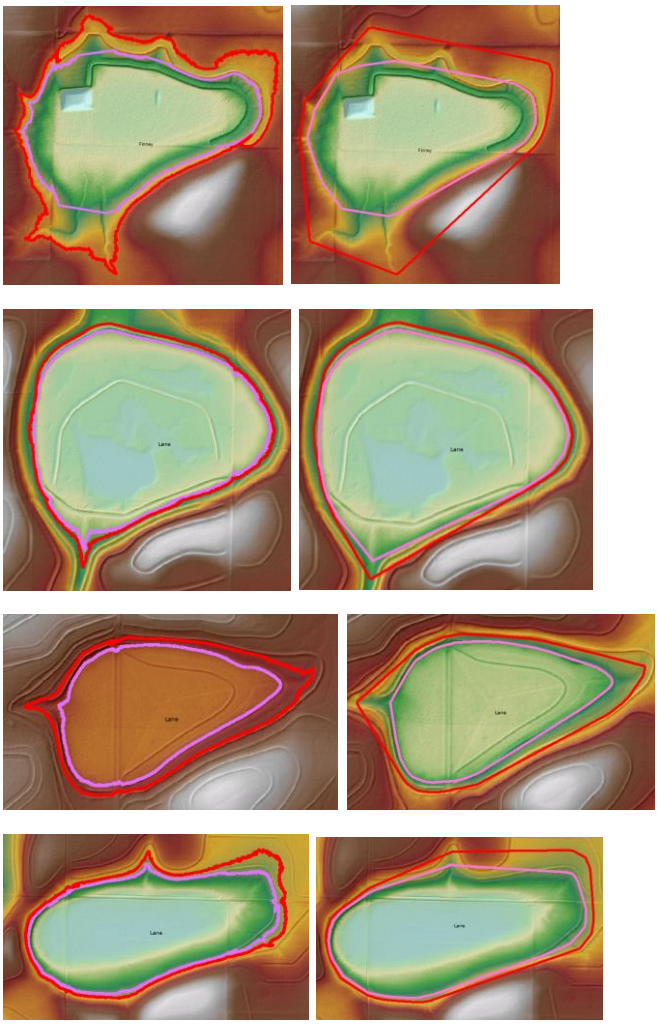

Figure 37. Outliers for OS vs SS MBG playa orientation

Playas 26, 50, 55, and 56; left: features mapped, right: MBG envelopes